Chemostratigraphy of the uppermost Cambrian at the Ordovician GSSP

by

Lisha Wang, BEng.

Brock University

Submitted in partial fulfillment of the requirements

for the degree of

Master of Science in Earth Sciences

Faculty of Mathematics and Science, Brock University

St. Catharines, Ontario

Abstract

Chemostratigraphy is an important tool for correlating layered sedimentary rock successions. Preserved/near primary carbon isotope signatures in marine carbonates can provide high-resolution profiles for sedimentary sequences supplementing the need for distinguishing fossils from different depositional environments and those lacking fossil materials.

The Global Boundary Stratotype Section and Point (GSSP) of the Cambrian–Ordovician boundary is located at Green Point in the Green Point Formation of the Cow Head Group in western Newfoundland, Canada. To reconstruct a continuous and high-resolution chemostratigraphy from the Cambrian–Ordovician boundary to the Furongian Series Stage 10, we included the $\delta^{13}C$ results of the Green Point Formation covering the Ordovician GSSP interval (Azmy et al., 2014).

The Green Point Formation through the base of Ordovician GSSP consists of alternating dark gray to black shale and thin ribbon limestone rhythmites, with few fossils. The samples are micritic limestone, dolomitic limestone, and dolostone. They were determined to be in primary to near-primary condition based on multiple screening tests. Cathodoluminescence screening reveals dull to bright luminescence of the samples indicative of good preservation for many of them. The $\delta^{13}C_{carb}$ and $\delta^{18}O$ values of the Green Point carbonates range from -6.44‰ to +0.33‰ (VPDB) and from -8.63‰ to -5.67‰ (VPDB), respectively, with poor correlation. Mn/Sr ratios range from 0.63 to 9.82, with no correlation to $\delta^{13}C_{carb}$, but with ratios supporting the near primary nature of the $\delta^{13}C$ values.

Carbon isotope compositions of the Green Point Formation below the Ordovician GSSP fluctuate but remaine essentially invariantly negative. The $\delta^{13}C$ values reveal a

negative excursion at and below the Cambrian–Ordovician boundary, which may correlate with the Top of Cambrian Carbon Isotope Excursion (TOCE) and its significant negative excursion. A nadir of -6.44 ‰ at the base of the *Eoconodontus* conodont zone marks the proposed GSSP for the base of the Furongian Series Stage 10. The lower excursion may be correlated with the Hellnmaria-Red Tops Boundary (HERB) carbon isotope excursion found in sequences in the United States of America, Australia, and north China. Without an adequate record of conodonts, high-resolution chemostratigraphic trends of carbon isotope compositions facilitate the correlation of intercontinental and intracontinental sequences.

Key words: Ordovician GSSP, carbon isotope values, Cambrian–Ordovician, Newfoundland, chemostratigraphy,

Acknowledgements

The author would like to thank Marty Ouellette for help with making thin sections, and Mike Lozon for editing some figures, and Karem Azmy (Memorial University of Newfoundland) for providing the samples, and for the carbon and oxygen isotope analyses. This research was financially supported by grants from the Natural Sciences and Engineering Research Council of Canada (NSERC 7961-215) to Uwe Brand.

Table of Contents

List of Tables

List of Figures

List of Abbreviations

Ave = average value

Ca = Calcium

CL = cathodoluminescence

COBWG = International Working Group on the Cambrian–Ordovician Boundary

C–O = Cambrian–Ordovician

FAD = first appearance datum

Fe = Iron

GSSP = Global Boundary Stratotype Section and Point

HERB = Hellnmaria-Red Tops Boundary

ISCS = International Subcommission on Cambrian Stratigraphy

ISOS = International Subcommission on Ordovician Stratigraphy

Max = maximum value

Mg = Magnesium

Min = minimum value

Mn = Manganese

N = number of samples

NBS = National Bureau of Standards (NIST)

NFLD = Newfoundland

ppm = parts per million (μg/g)

Sr = Strontium

TOCE = Top of Cambrian Excursion

VPDB = Vienna Pee Dee Belemnite

Chapter 1
Introduction

In 1999, the Ordovician Global Boundary Stratotype Section and Point (GSSP) was located in the Green Point section (western Newfoundland, Canada) by the International Working Group on the Cambrian–Ordovician Boundary (COBWG) after investigating it for 25 years (Figure 1; Cooper et al., 2001). The Green Point section satisfied the criteria required of global boundary stratotype sections, such as: 1) continuity of sedimentation through the boundary interval, 2) completeness of exposure, 3) adequate thickness of exposure, 4) abundance and diversity of well-preserved fossils, 5) favourable facies for development of widespread reliable and time-significant correlation horizons, 6) freedom of structural complication, metamorphism, and other alteration, 7) free of unconformities, 8) amenability to magnetostratigraphy and geochronometry, and 9) accessibility (Barnes, 1988). Compared with other GSSP candidate sections, such as the Lawson Cove section in North America, the Black Mountain section in Australia, and the Dayangcha section in north China, the Green Point section is under-investigated for geochemistry with only informal and unpublished carbon isotope research done (Azmy et al., 2014; Cooper et al., 2001).

Chemostratigraphy can record general chemical changes of sea water and variation of sea level that can affect a wide area and coeval deposition would record the same variations. Therefore, chemostratigraphy is a useful tool for correlating and subdividing global rock sequences. Since carbon is the most important element in calcium carbonate, the preserved/near primary stable carbon isotope signature in marine carbonates can provide

high-resolution profiles for sedimentary sequences eliminating the need for distinguishing fossils from different depositional environments (Azmy et al., 2014).

The strata of the Cambrian–Ordovician boundary belong to the Martin Point Member, Green Point Formation, Cow Head Group that consists of green shale and ribbon limestone with scarce fossils. Therefore, carbon isotopes from whole rock is a better proxy than brachiopods and conodonts which are widely used in Paleozoic strata, but are rarely preserved in the Green Point section (James and Steven, 1986; Brand et al., 2011). In fact, the inorganic-carbonate carbon-isotope composition has received more attention than the organic carbon isotope one (e.g., Ripperdan et al., 1992; Terfelt et al., 2014). At Green Point of western Newfoundland, Azmy et al. (2014) build an inorganic carbon isotope profile of the Ordovician GSSP interval, and we will continue Azmy et al's work and build a high-resolution $\delta^{13}C_{carb}$ profile from the Cambrian–Ordovician boundary to the bottom of the Cambrian System Furongian Series Stage 10, and correlate the Green Point interval with other sections covering the Cambrian–Ordovician boundary interval around the world.

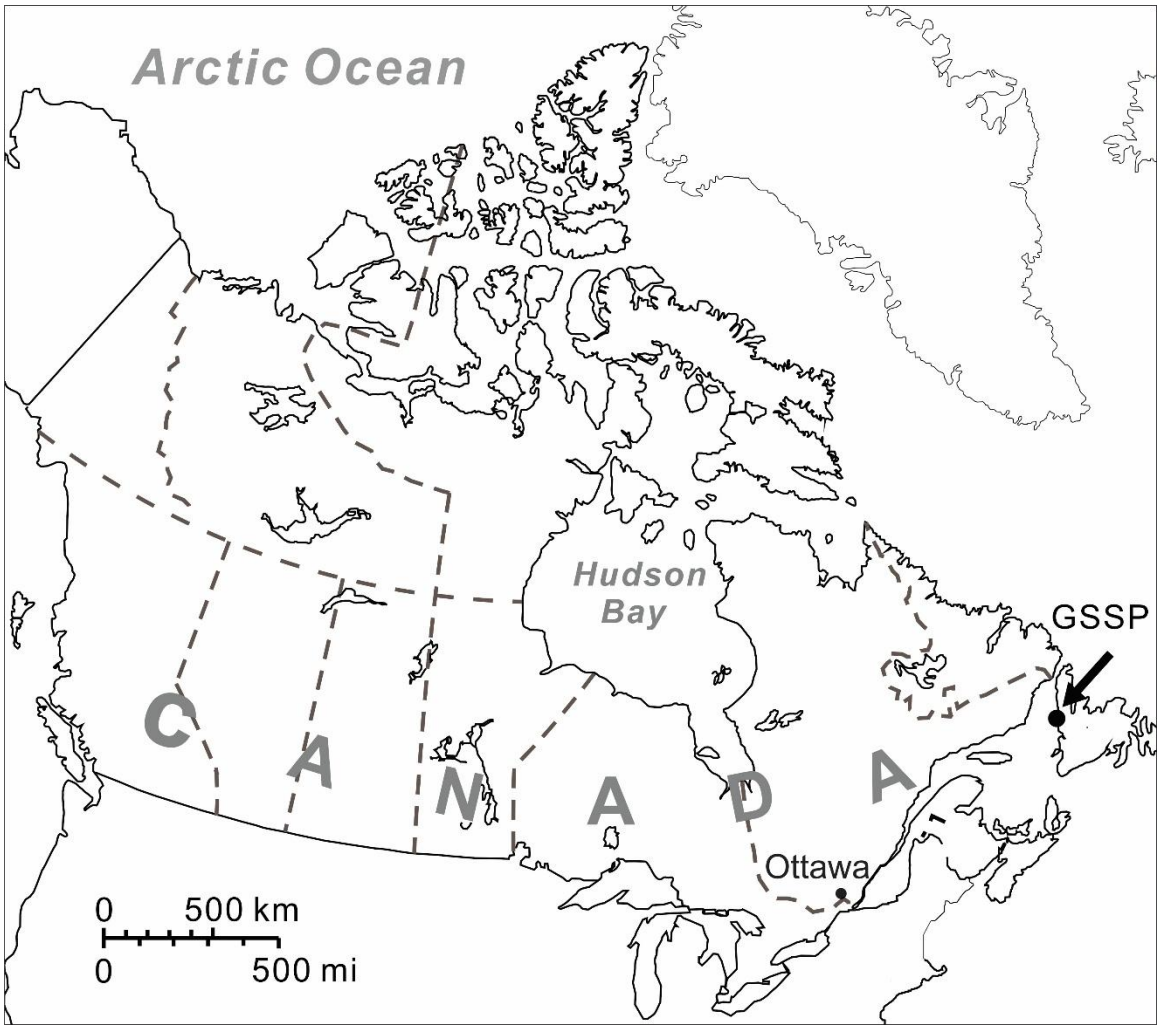

Figure 1. Location of the Ordovician GSSP in western Newfoundland, Canada (modified from Azmy et al., 2014)

Chapter 2

Geological Setting

2.1 Sedimentology

The strata of the Cambrian–Ordovician boundary belong to the Martin Point Member of the Green Point Formation of the Cow Head Group (James and Steven, 1986). Thirty years ago, James and Steven (1986) did a comprehensive investigation of the stratigraphy and a local correlation of the Cambrian–Ordovician Cow Head Group in western Newfoundland. Here is a short summary:

The Cow Head Group is exposed widely in western Newfoundland and sediments accumulated on the platform during transgression of the eastern Laurentian margin (Figure 2) around 570–550 Ma years ago (James and Steven, 1986). The group spans around 70 million years from the late Middle Cambrian to early Middle Ordovician and consists of a 300–500 m thick sequence of carbonate and shale (James and Stevens, 1986). The Cow Head Group is exposed as a klippe overlying Middle Ordovician red shale and volcanogenic sandstone (James, 1981; Suchecki and Hubert, 1984; Williams et al. 1985). The facies and lithologies of the Cow Head Group vary from location to location and two major contemporaneous formations are recognized. The coarse-grained, conglomerate forms the Shallow Bay Formation, whereas the fined-grained shale is the Green Point Formation (James and Stevens, 1986).

The Green Point Formation at the base of the slope represents the most distal part of the carbonate apron with shale, ribbon limestone and scarce conglomerate (Cooper et al., 2001; James and Stevens, 1986). The upper unit, St. Paul's Member consists mostly of red shale. The middle Broom Point Member consists of ribbon limestone and conglomerate.

The basal Martin Point Member varies from 100 to 150 m is green and black shale, with thin buff-weathering siltstone and layers or packages of ribbon limestone and a few thin layers of conglomerate (James and Stevens, 1986; Figure 4).

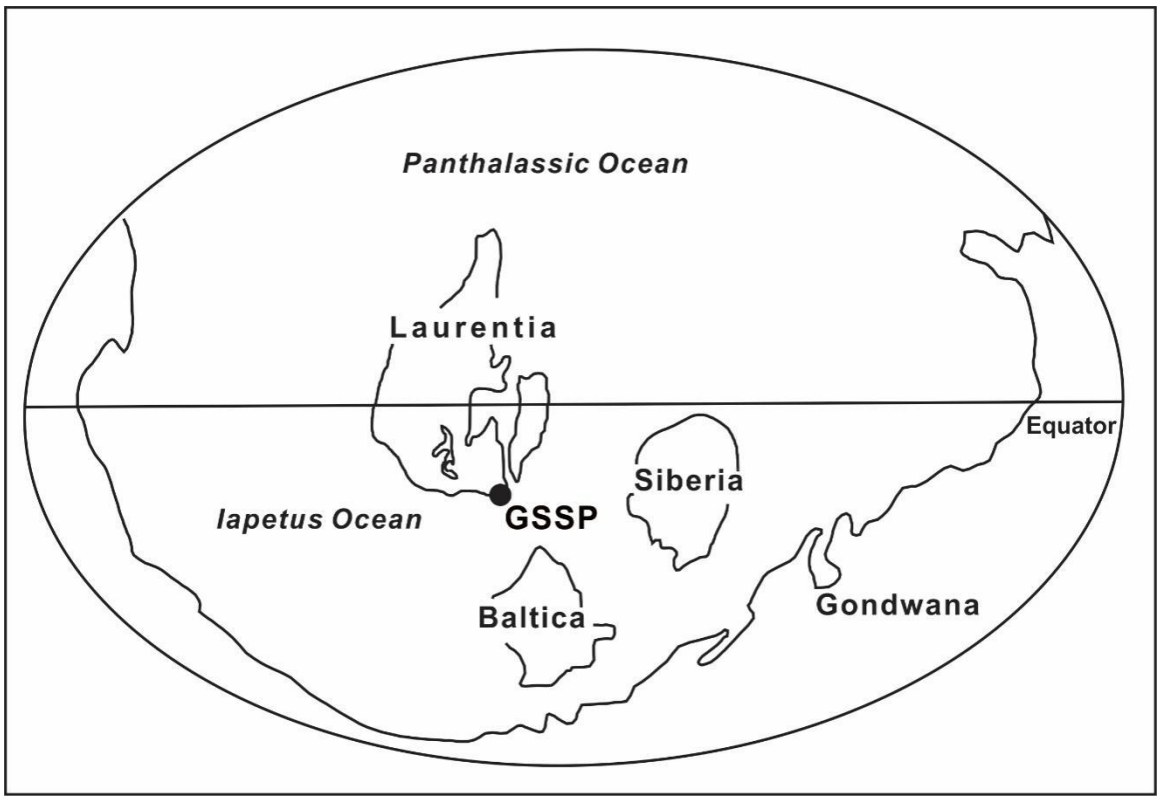

Figure 2. Location of the Ordovician GSSP on the Paleomap (modified from Scotese, 2002, PALEOMAP Project, http://www.scotese.com).

The spike designating the Cambrian–Ordovician boundary is located within Bed 23 which is the lowest bed of the Broom Point Member at Green Point (Cooper et al., 2001). Therefore, the beds below the Ordovician GSSP belong to the Martin Point Member (Figures 3, 4). The Martin Point Member at Green Point was measured and described in detail by James and Steven (1986). It consists of green shale, siltstone, ribbon limestone, lime mudstone, and minor conglomerate (Figure 4). Our samples were obtained from limestone layers of Beds 17 to 3(c) (Figures 3, 5).

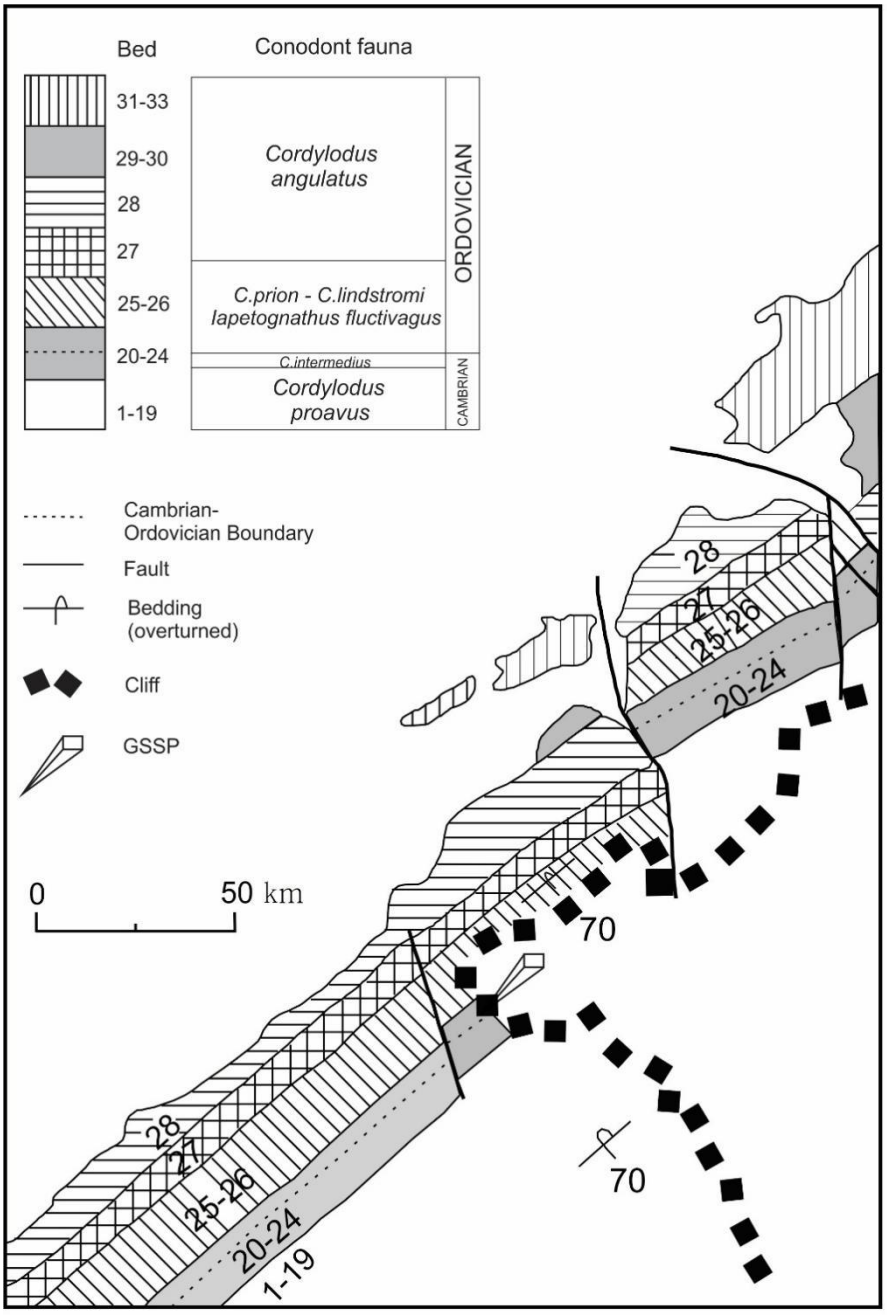

Figure 3. Map of Green Point, western Newfoundland, Canada showing the distribution of outcrops of the beds that bracket the Cambrian–Ordovician boundary interval (modified from Cooper et al., 2001).

2.2 Paleontology and Biostratigraphy

During the Cambrian, trilobites were common and distinguishable fossils extremely useful for worldwide biostratigraphic correlation (Palmer, 1977). The FAD First appearance datum) of *Lotagnostus americanus* was approved by the ISCS in 2004 as a potential indicator for the base of the Furongian Series Stage 10 (Babcock, 2005). Most Cambrian trilobites of the Cow Head Group are found in conglomerates or shallow-water limestones of the Shallow Bay Formation (James and Steven, 1986). At Green Point, trilobite fossils are rarely found in the deep-water Green Point Formation. Therefore, trilobites cannot be used to correlate Cambrian–Ordovician sections.

In the late Cambrian, however, conodonts are reliable for correlating carbonate sequences (Table 1; Azmy et al., 2014; Cooper et al., 2001; Terfelt et al., 2012). The FAD of *Iapetognathus fluctivagus* marks the Ordovician GSSP within Bed 23 at Green Point (Cooper et al., 2001). The strata under the Cambrian–Ordovician boundary span the *Cordylodus intermedius* to *Eoconodontus notchpeakensis* biozones, but there is no conodont record under the *E. notchpeakensis* biozone.

E. notchpeakensis can be easily recognized by its two-element apparatus (Landing et al. 2010; Terfelt et al., 2012). The FAD of the conodont *E. notchpeakensis* at the onset of the HERB excursion is the proposed GSSP for the base of Cambrian Stage 10 (Landing et al., 2010, 2011, Miller et al., 2011, 2015), which is easily recognizable across Laurentia, east and west Gondwana, central Asia and Baltica (Landing et al. 2011; Terfelt et al., 2012). At Green Point, it is difficult to subdivide and correlate sections for the lack of fossils. In contrast, carbon isotope chemostratigraphy is a valuable and important tool that can compensate for this lack of suitable fossil material (Azmy et al., 2014).

Table 1. Correlation of conodont biozones for the Cambrian–Ordovician interval on Laurentia with North and South China (modified from Azmy et al., 2014; based on Cooper et al., 2001; Terfelt et al., 2012).

System	Laurentia			North China		South China
	GSSP	Lawson Cove		Dayangcha		Hunan
ORDOVICIAN	*Cordylodus angulatus*	*Cordylodus angulatus*	Fauna B	*Cordylodus angulatus-Chosonodina herfurthi*		*Cordylodus angulatus*
	Iapetognathus fluctivagus	*Iapetognathus*	Fauna B	*Cordylodus lindstromi*		*C.lindstromi*(upper part)-*Iapetognathus fluctivagus*
		Cordylodus lindstromi s.l.	Fauna B			*Cordylodus lindstromi* (lower part)
CAMBRIAN	*Cordylodus intermedius*	*Cordylodus intermedius*: *Clavohamulus hintzei*; *Hirsutodontus simplex*	Fauna A	*Cordylodus intermedius*		*Cordylodus intermedius*
	Cordylodus proavus	*Cordylodus proavus*: *Clavohamulus elongatus*; *Fryxellodontus inomatus*; *Hirsutodontus hirsutus*	Fauna A	*Cordylodus proavus*		*Cordylodus proavus*
	Eoconodontus notchpeakensis	*Eoconodontus*: *Cambrooistodus minutus*; *Eoconodontus notchpeakensis*		*Cambrooistodus*		*Eoconodontus*
	no record	*Proconodontus muelleri*		*Proco-nodontus*	*Proconodontus muelleri*	*Proconodontus*

Chapter 3

Methods

Ninety-six samples were collected from Beds 3(c) to 17 below the Cambrian–Ordovician boundary (49° 40’ 51” N; 57° 57’ 36” W) at Green Point, western Newfoundland. The samples are taken from laminated limestone to avoid allochthonous clasts (Figures 4.1, 4.2).

The carbonate samples were split into three parts using a rock saw, and two thin sections were made for each sample. The first thin section of the first split was used for petrographic analyses with a polarizing microscope. They were cut to a thickness of 30 μm and half of each was stained with Alizarin Red-S and potassium ferricyanide solution (Dickson, 1966; Lindholm and Finkelman, 1972). The second set of thin sections was cut to a thickness of 50 μm and used for cathodoluminescence (CL) observations. The Nuclide 3 LM Cathode Luminoscope was operated with an average 10.98 kV accelerating voltage and 0.82 mA current (Brock University).

The powder for trace element and stable isotope analyses was drilled from the fine grained limestone on the mirror-image slab of the CL thin section using a dental drill. It was guided by petrographic and CL observations to avoid recrystallization, cementation and other contaminants. For each sample, one or more spots were chosen for drilling and around 20 mg of powder was weighed out to four decimal places with a Sartorius balance and subsequently stored in a 10 mL clean tube. 7.3 mL of 2.1 % (v/v) distilled HNO_3 was added into each tube for digesting the powder with a Hamilton MicroLAB 600 Series diluter. After more than 12 hours each sample solution was filtered to remove the insoluble residue. Clean sample solutions were used to analyze for Ca, Mg, Mn, Sr, and Fe content

using the Varian SpectrAA 400P atomic absorption spectrometer at Brock University. The carrier gas for the Sr test was nitrous oxide, whereas for all the others we used acetylene. All elemental results were normalized to a 100 % carbonate basis (cf. Brand and Veizer, 1980). The reproducibility (accuracy and precision) of the results was monitored by the analysis of NIST standard reference material NBS 633 (N=103) throughout the chemical analyses. The percent reproducibility was 2.12 % for Ca, 1.76 % for Mg, 3.03 % for Sr, 4.7 % for Mn, and 5.25 % for Fe with respect to certified NBS values.

For stable carbon and oxygen isotope analyses, the experiments were carried out on a Thermo-Finnigan DELTA V GasBench II coupled to a TF DELTA V isotope ratio mass spectrometer at Memorial University of Newfoundland. The powders were reacted with 100% orthophosphoric acid at 70 ℃. Uncertainty of the analyses was better than 0.1 ‰ (2σ) of NBS 19. The stable carbon and oxygen isotope compositions are expressed in the conventional $\delta^{13}C$ and $\delta^{18}O$ notations relative to Vienna Pee Dee Belemnite (VPDB).

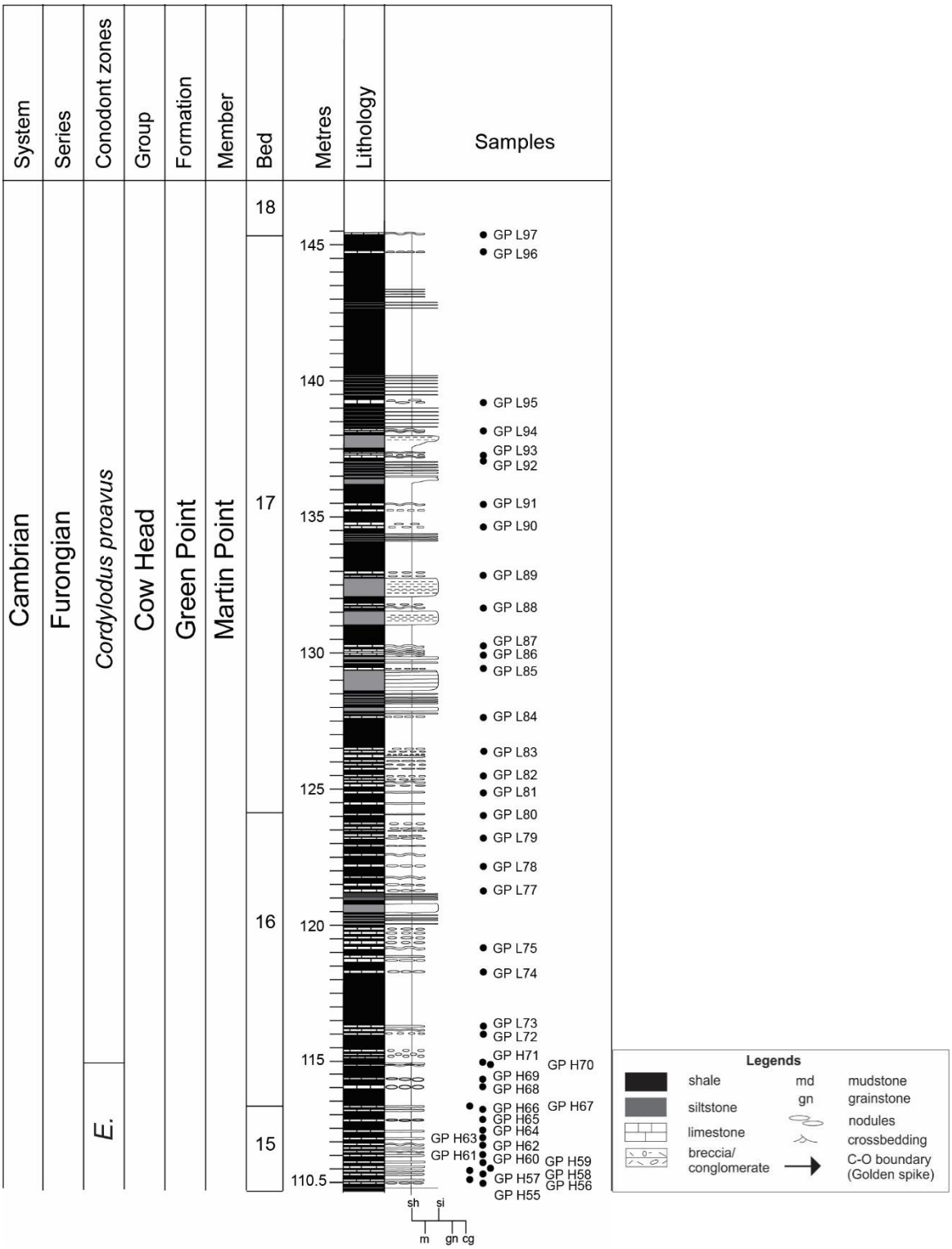

Figure 4.1 Stratigraphic framework of Bed 15 to 18 below the Cambrian–Ordovician boundary at Green Point, western Newfoundland, Canada. It details bed numbers and measured positions of investigated samples and the conodont zonation scheme (modified from Cooper et al., 2001; James and Steven, 1986).

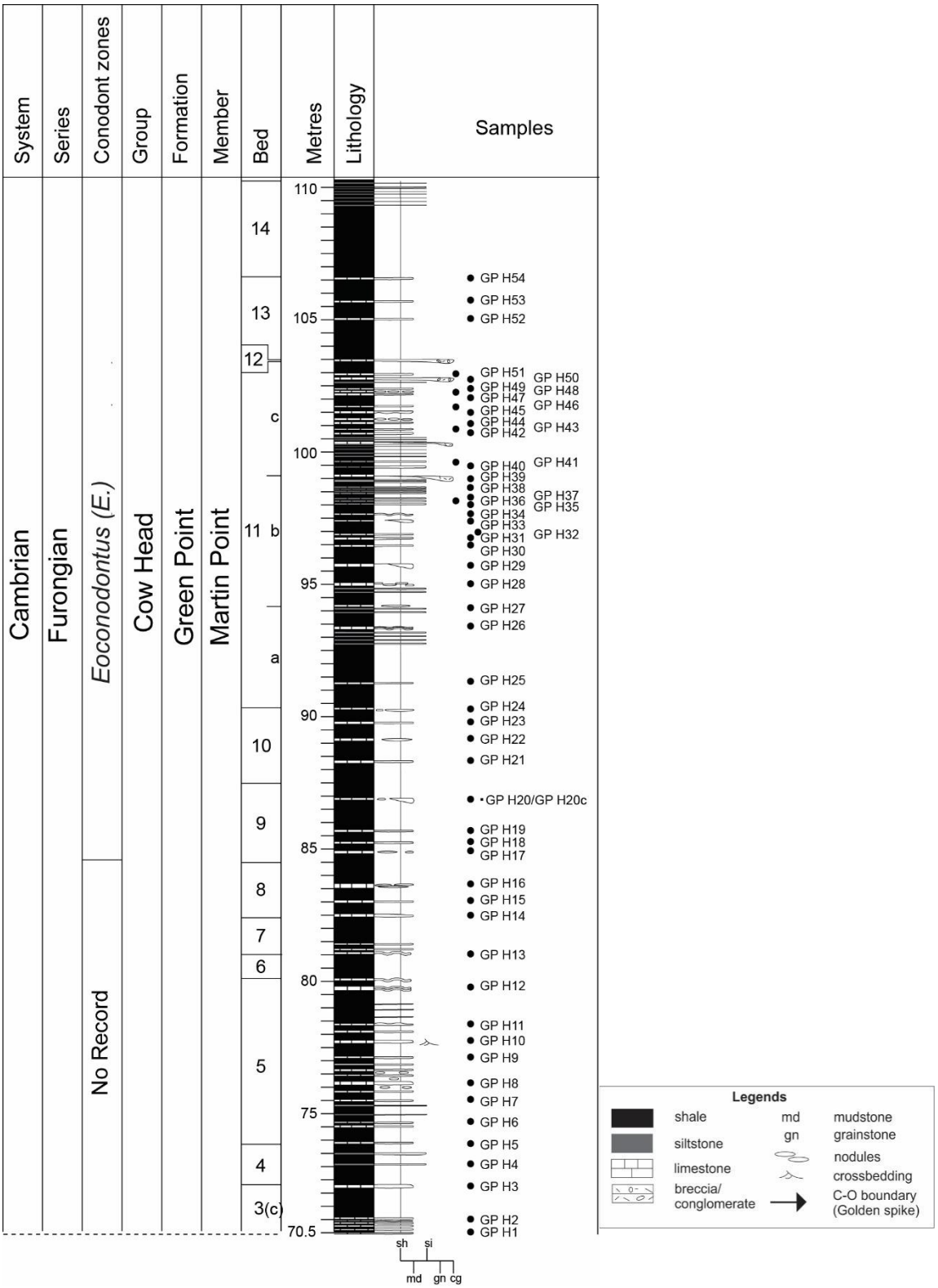

Figure 4.2 Stratigraphic framework of Bed 3(c) to 14 below the Cambrian–Ordovician boundary at Green Point, western Newfoundland, Canada. It depicts bed numbers and measured positions of investigated samples, and the conodont zonation scheme (modified from Cooper et al., 2001; James and Steven, 1986).

Chapter 4

Results

4.1 Petrography

At Green Point, our carbonate samples are dominantly limestone that stained red (Figure 5). Tiny carbonate particles were produced in great abundance and accumulated on the bottom of the sea floor wherever turbulence was insufficient to put them in suspension and currents were too weak to carry them away.

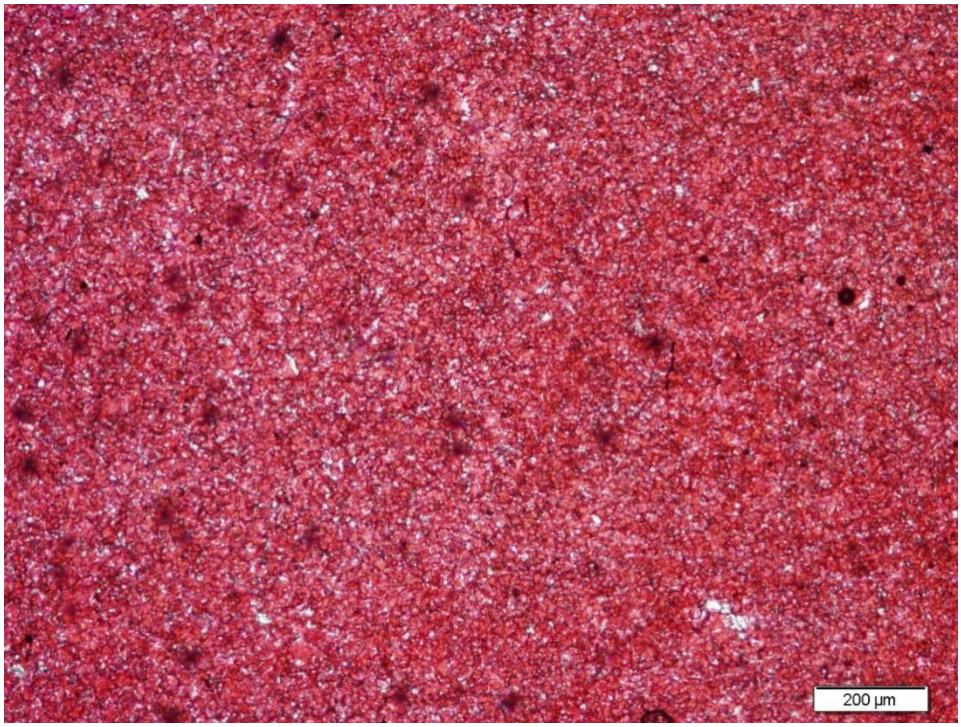

Figure 5. Photomicrograph of sample GP H66 (under plane-polarized light).

Rhombohedra of dolomite and ferroan dolomite were noted in some samples. Twelve samples are dolomitic limestone in which rhombic dolomite grains deposited without being stained (Figure 6). In three samples, the matrix was replaced by ferroan dolomite which stained blue with potassium ferricyanide solution (Figure 7). The euhedral dolomite

crystals can be easily distinguished from the anhedral calcite and angular quartz sand. At Green Point, rhombic dolomite crystals have a turbid center surrounded by a clearer rim. They usually contain minute calcite inclusions which stained red. In dolomitic limestones, crystals composed chiefly of dolomite and quartz are in irregular contact with the calcitic matrix. The dolomite and quartz occur in laminated beds that alternate with others consisting solely of calcite. Alternating laminations of dolomite and calcite perhaps are caused by changing physicochemical conditions in the depositional environment favouring early dolomitization of some layers and not of others. Dolomite contains angular quartz sand grains inherited from original calcarenites whose textures have been obliterated by dolomitization; in some of these rocks the quartz grains are deposited in cross-laminae, indicating that limestone deposition was affected by currents.

Pressure solution and recrystallization were noted in some samples. Sample GP H51 contains enlarged and bend calcite grains growing upwards (Figure 8). In sample GP L70, quartz replaced the calcite that was deposited as coarse sand (Figure 9). The micritic limestone samples (e.g., GP H66) also show an upgrade trend in a few of samples (Figure 10). Some samples show layers which were formed by algae and quartz (Figures 11, 12). Fifteen samples show pyrite that are scattered or banded in the samples (Figure 13).

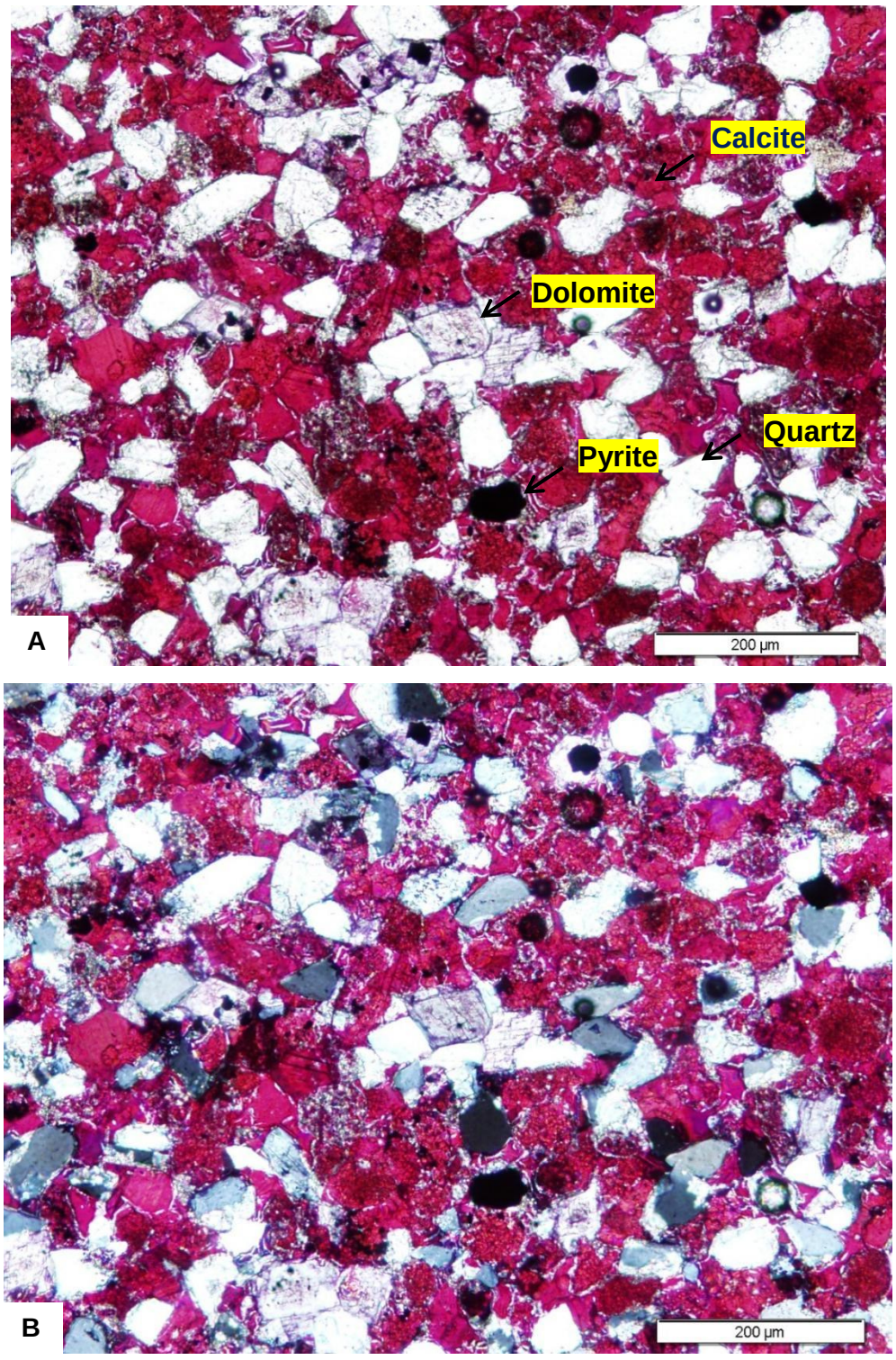

Figure 6. Photomicrographs of sample GP H18 (dolomitic limestone): (A) under plane-polarized light; (B) under cross-polarized light. The calcite crystals are partially replaced by dolomite crystals.

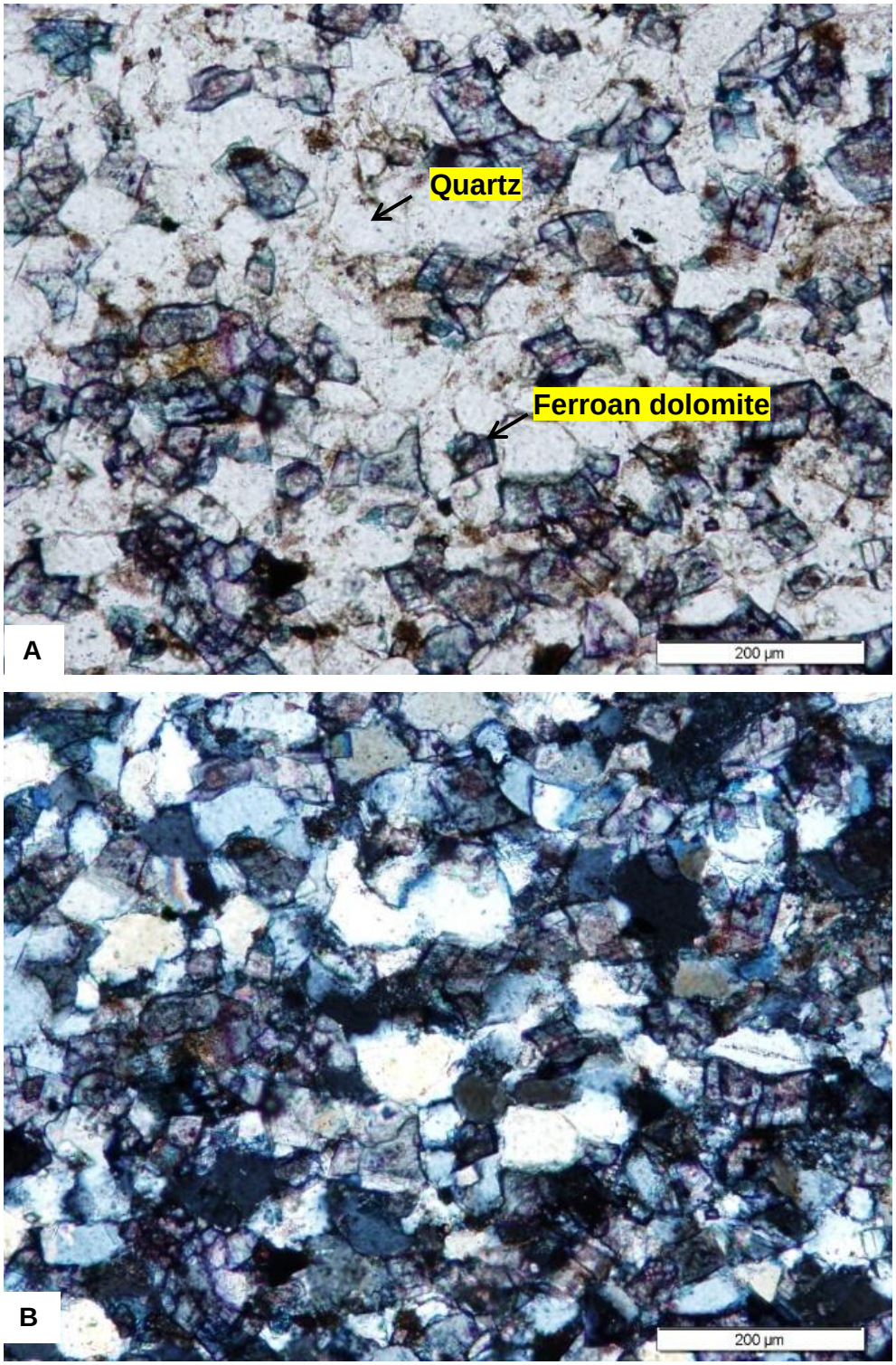

Figure 7. Photomicrographs of sample GP H5 (ferroan dolomite): (A) under plane-polarized light; (B) under cross-polarized light. It is completely dolomitized by ferroan dolomite with some angular quartz sand.

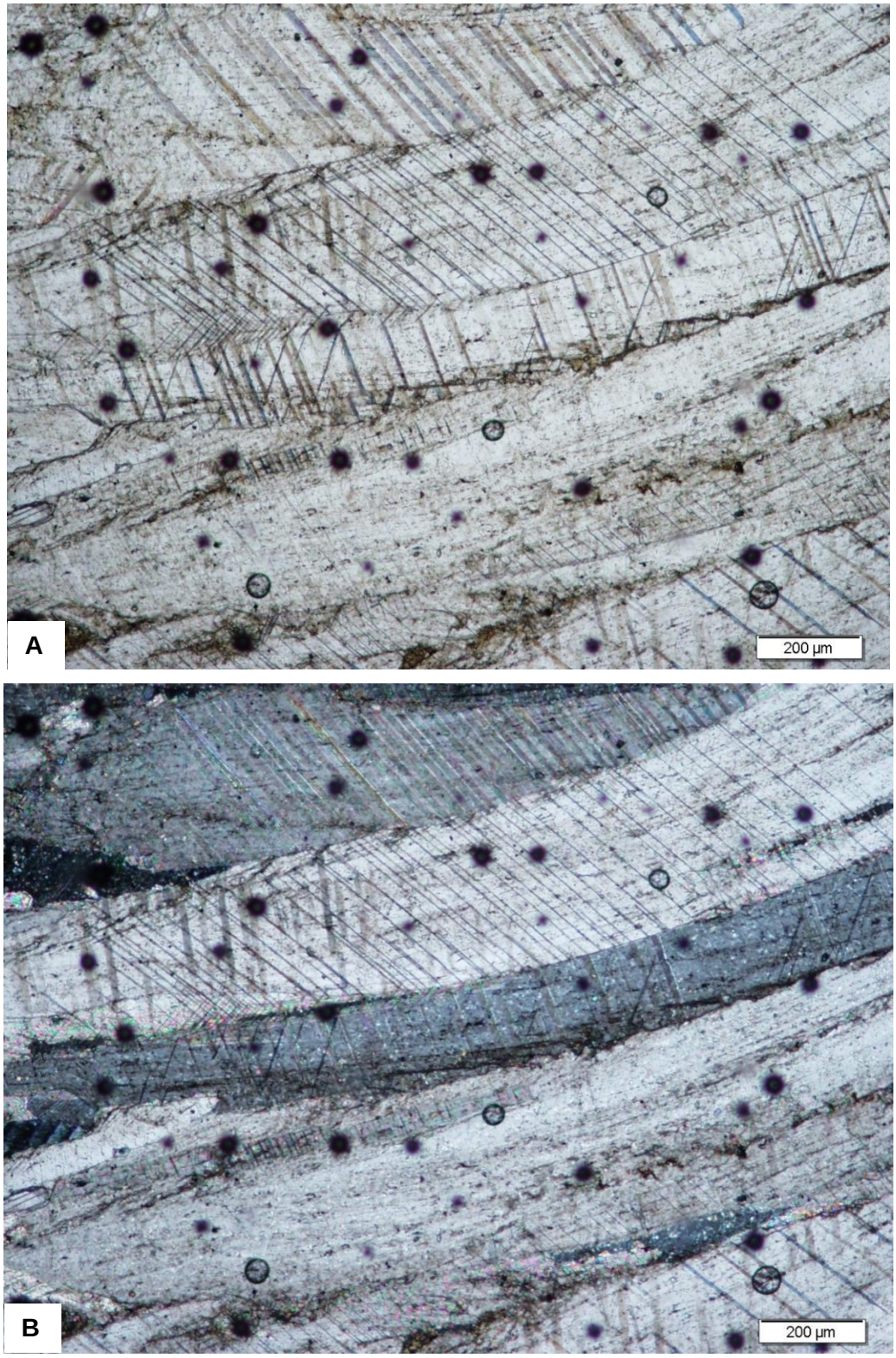

Figure 8. Photomicrographs of sample GP H51: (A) under plane-polarized light; (B) under cross-polarized light. Bent calcite sand shows signs of pressure solution (dark bands).

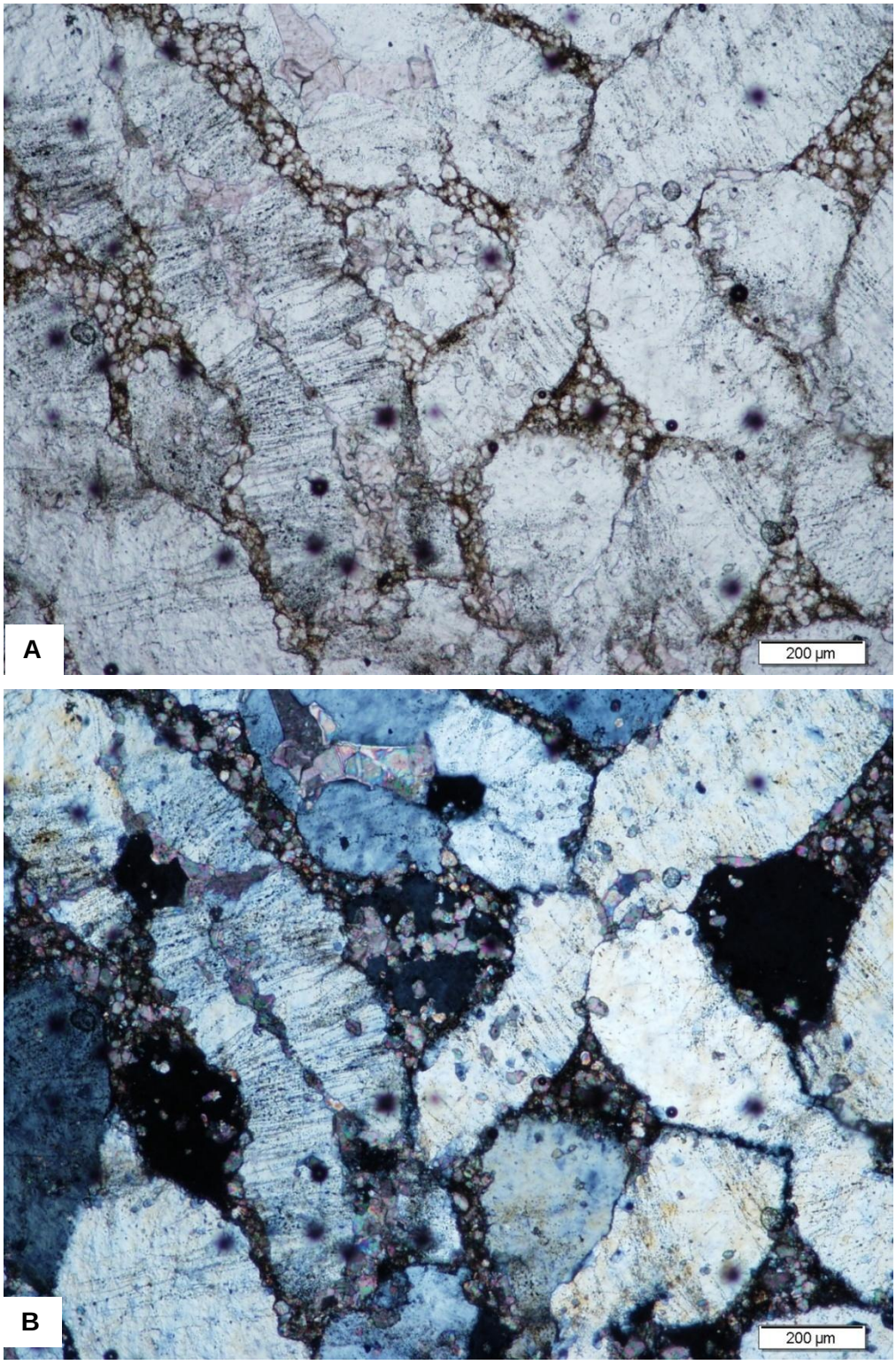

Figure 9. Photomicrographs of sample GP H70; (A) under plane-polarized light; (B) under cross-polarized light. It shows quartz replacement.

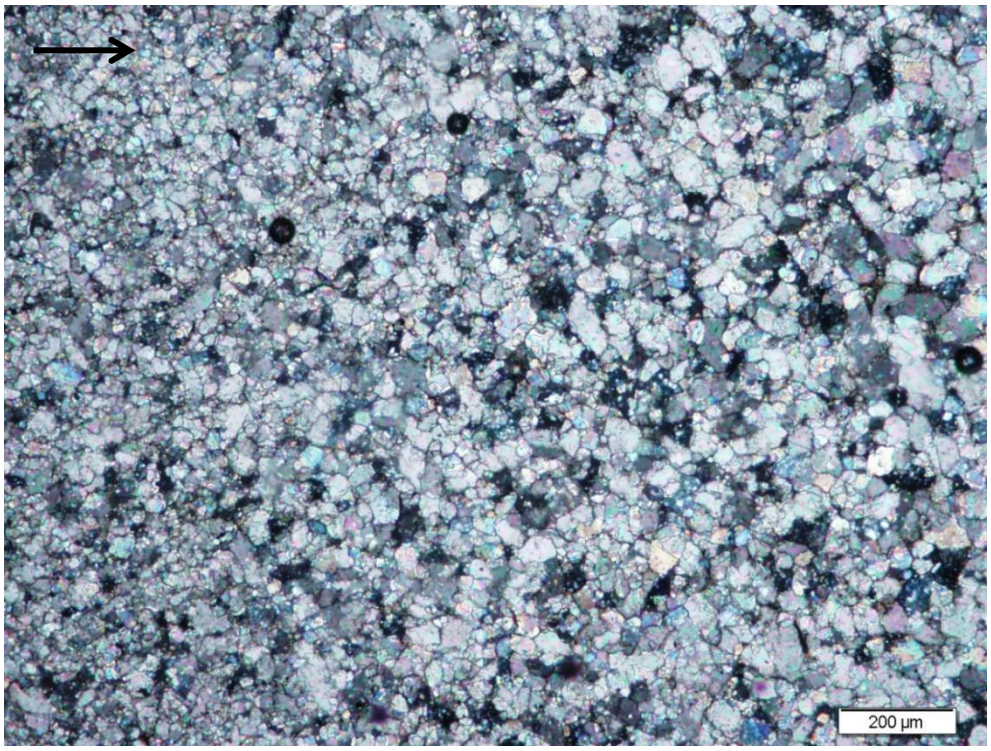

Figure 10. Photomicrograph of sample GP H66 (under cross-polarized light). It shows aggrading calcite grains.

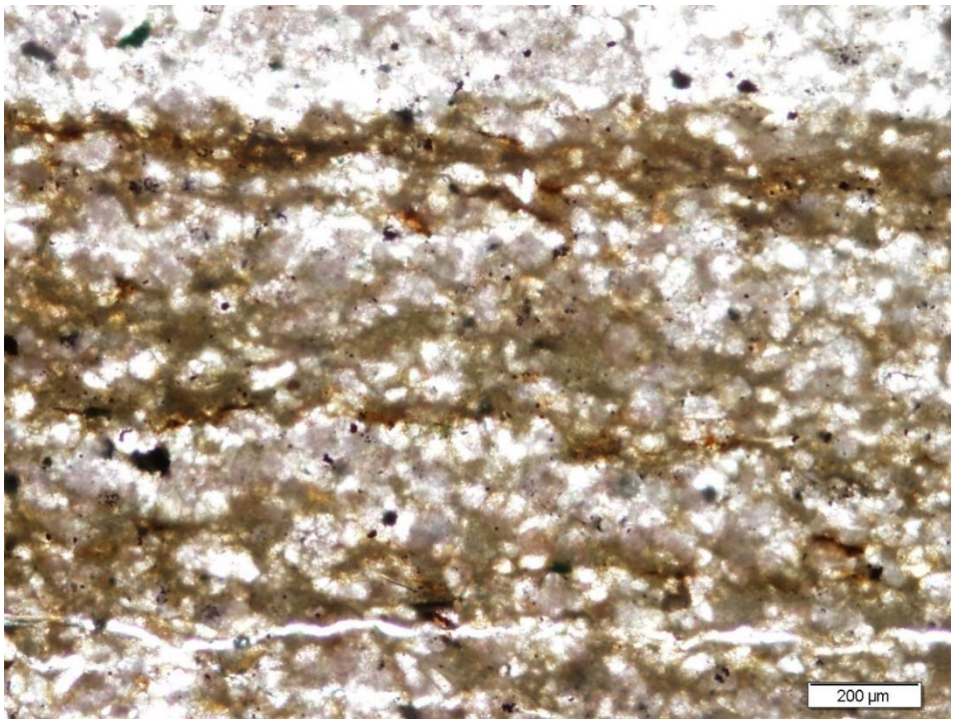

Figure 11. Photomicrograph of sample GP H17 (under plane-polarized light). It shows algae layers.

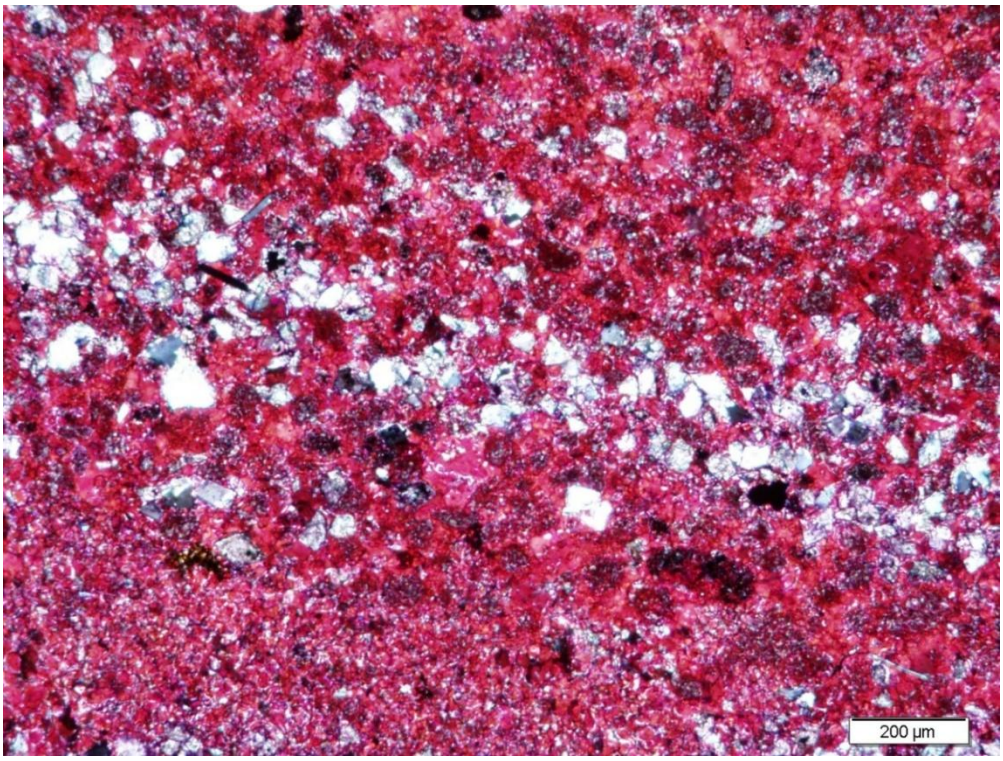

Figure 12. Photomicrograph of sample GP H77 (under cross-polarized light). It shows one quartz layer.

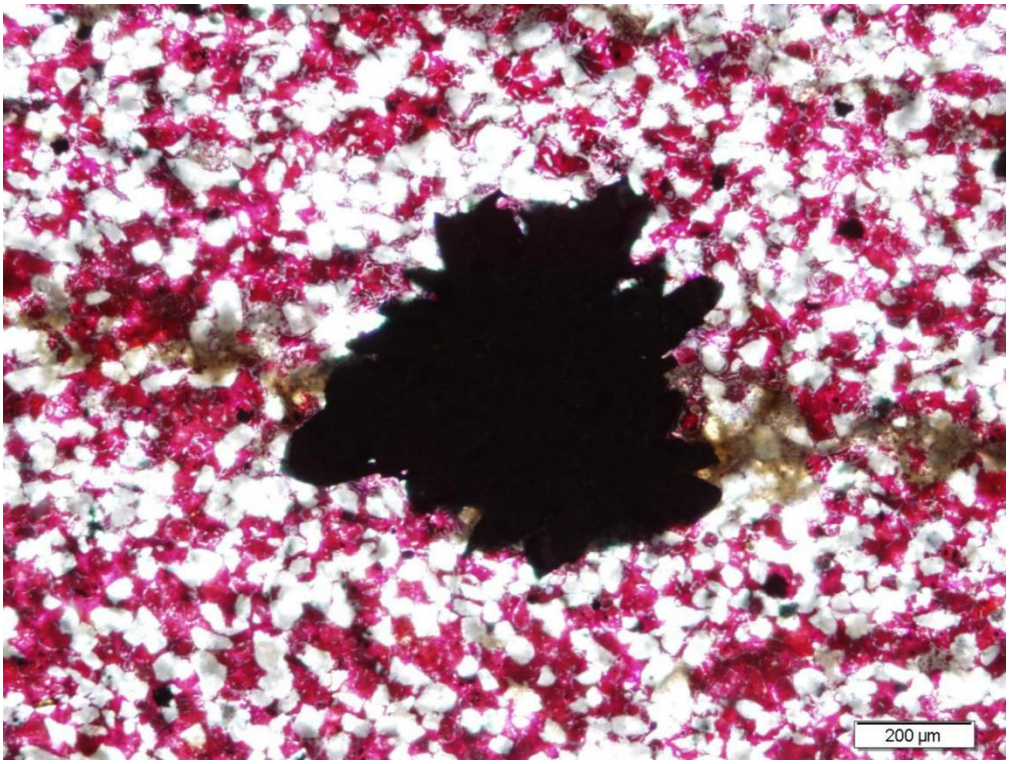

Figure 13. Photomicrograph of sample GP H17 (under cross-polarized light). The black patch in the middle is a pyrite grain.

4.2 Cathodoluminescence

Cathodoluminescence aids in the evaluation of the preservation status of carbonates. Dull cathodoluminescence, in general, indicates relative good preservation of geochemical signatures and bright cathodoluminescence may be caused by post-depositional diagenesis (Machel and Burton, 1991). In this research, 13 samples show dull cathodoluminescence (Figure 14). Sixty-six samples have dull red cathodoluminescence (Figure 15) and 29 samples have bright red-orange luminescence (Figure 16).

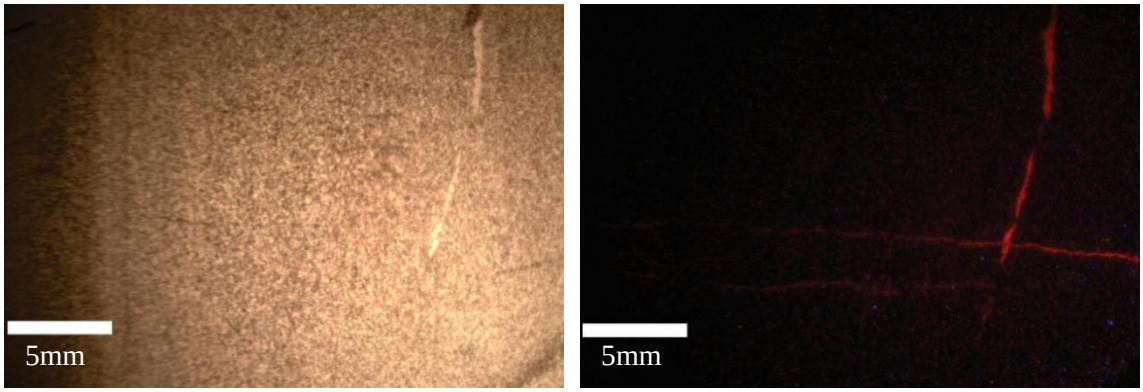

Figure 14. Cathodoluminescence of sample GP H6. It shows dull cathodoluminescence.

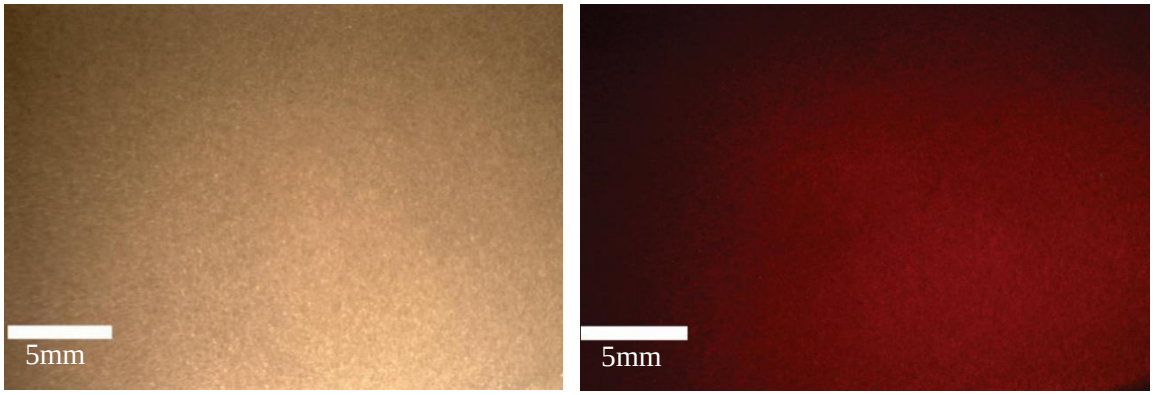

Figure 15. Cathodoluminescence of sample GP H55. It shows dull red cathodoluminescence.

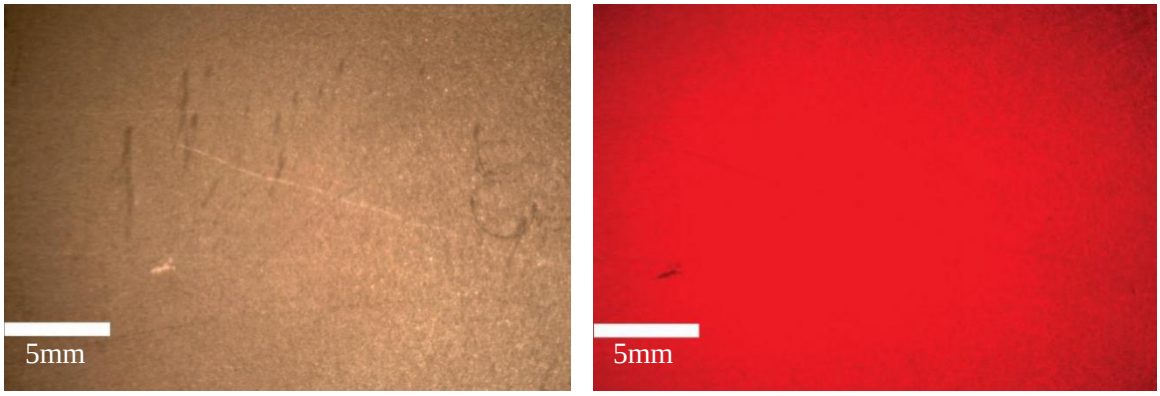

Figure 16. Cathodoluminescence of sample GP H23. It shows bright cathodoluminescence.

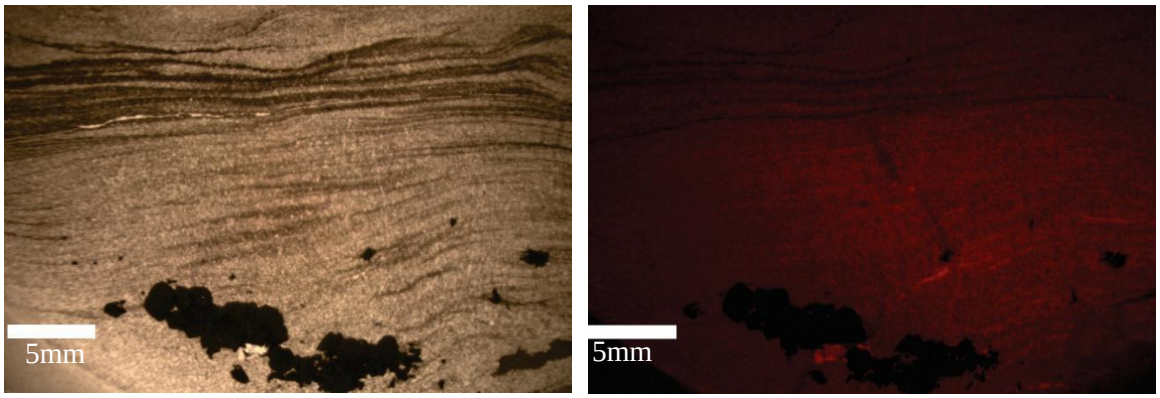

Figure 17. Cathodoluminescence of sample GP H17. Pyrite does not luminescence.

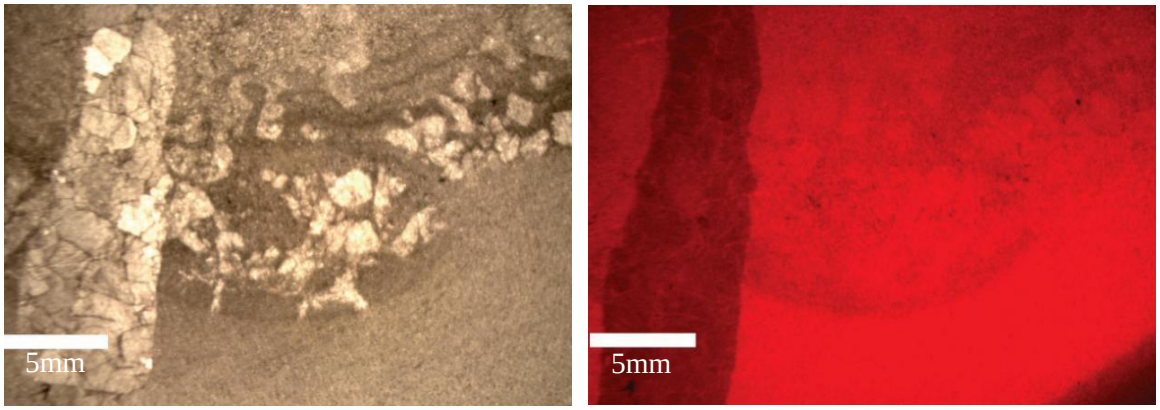

Figure 18. Cathodoluminescence of sample GP H25. The clasts have two different sources.

Some samples contain pyrite and as expected it does not luminesce (Figure 17). The pyrite may be scattered throughout the matrix or form layers within the carbonates. They also appear within algal layers that exhibit dull cathodoluminescence. Other samples contain clasts collapsed from shallow places that show different cathodoluminescence from the matrix (Figure 18). For trace element analysis, the powder of samples was always drilled from matrix avoiding acquisition from other sources such fracture and void-filling cement, weathered rinds, infilling and replacement materials.

4.3 Trace Elements

The trace element contents of the carbonate samples from the Green Point Section are tabulated in Appendix 1, and trends and distributions are illustrated in Figures 19–22. Based on petrographic evaluation, samples can be divided into three groups (Table 2). Calcium content decreases from limestone to dolostone, while Mg, Mn, and Fe contents increase with increasing dolomite concentration. Dolostone has low and stable Sr concentration, while limestone and dolomitic limestone contain, on average, more Sr. The Mn/Sr ratios are lower than 10 in all samples and the average Mn/Sr ratio also increases with increasing dolomite content (Figure 22).

Table 2. Chemical features of samples

Groups		**$\delta^{13}C$**	**$\delta^{18}O$**	**Ca**	**Mg**	**Sr**	**Mn**	**Fe**	**Mn/Sr**
		‰	**‰**	**ppm**	**ppm**	**ppm**	**ppm**	**ppm**	
Limestone	N	83	83	94	94	94	94	94	94
	Ave	-2.31	-7.60	390818	4182	298	611	2746	2.23
	Min	-6.44	-8.63	385780	1715	144	226	658	0.63
	Max	0.33	-6.92	393285	9220	953	2015	8663	9.82
Dolomitic-limestone	N	12	12	12	12	12	12	12	12
	Ave	-2.88	-7.38	327750	67251	295	994	23241	3.60
	Min	-4.82	-8.55	290646	13890	213	598	3918	1.25
	Max	-1.52	-6.86	381110	104354	478	1596	38151	5.83
Dolostone	N	3	3	3	3	3	3	3	3
	Ave	-1.97	-6.47	273707	121293	242	1383	27334	5.68
	Min	-2.12	-6.91	270146	114327	222	1047	12801	4.72
	Max	-1.77	-5.67	280673	124854	262	1644	38351	6.28

(N= number of samples; Ave: average value; Min: minimum value; Max: maximum value)

The Fe content of limestone is lower than 10,000 ppm. The dolomitic limestone and dolostone have high Fe with averages of 23,241 and 27,334 ppm, respectively. In general, the Mn content of dolomitic limestone and dolomite are higher than in limestone. The Fe content shows no clear correlation with Mn content in all samples (Figure 19).

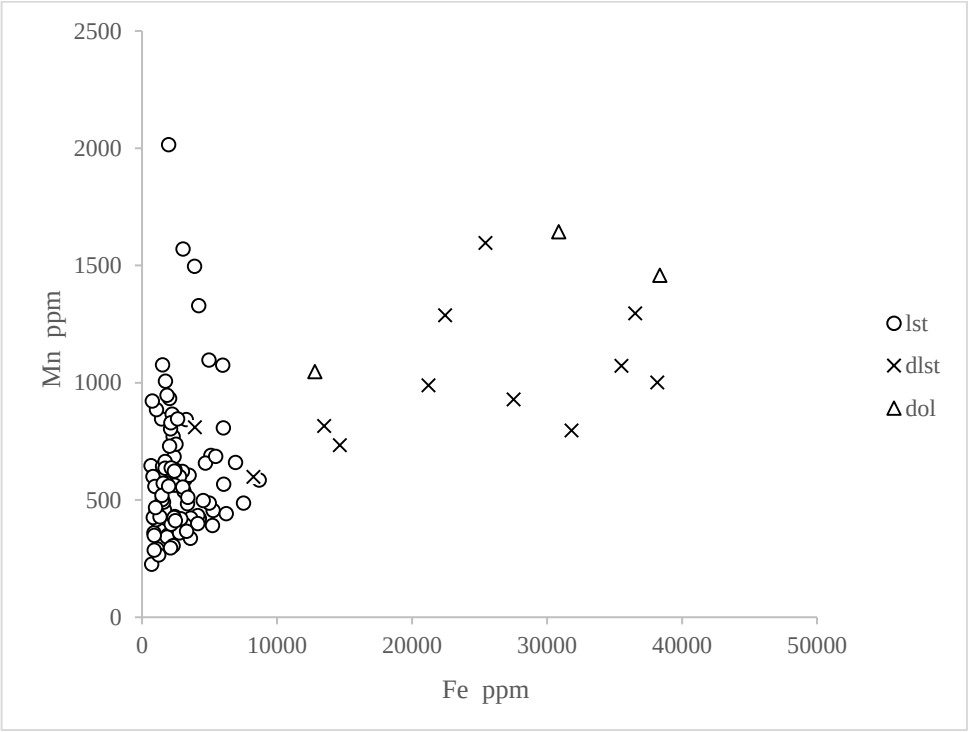

Figure 19. Scatter diagram showing the correlation of Mn with Fe.

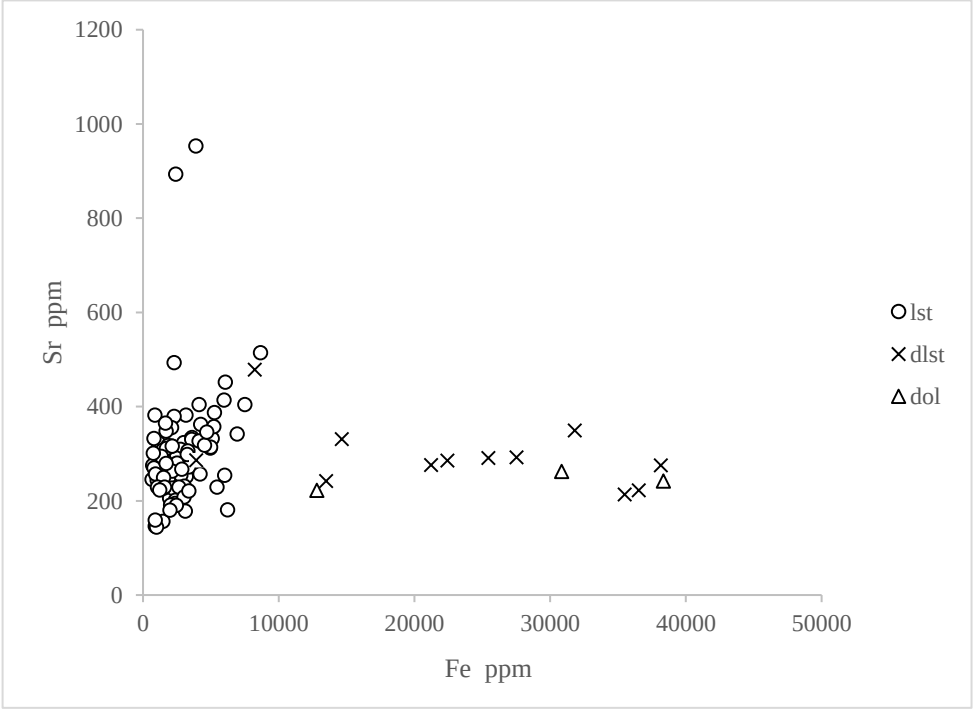

Figure 20. Scatter diagram showing the correlation of Sr with Fe.

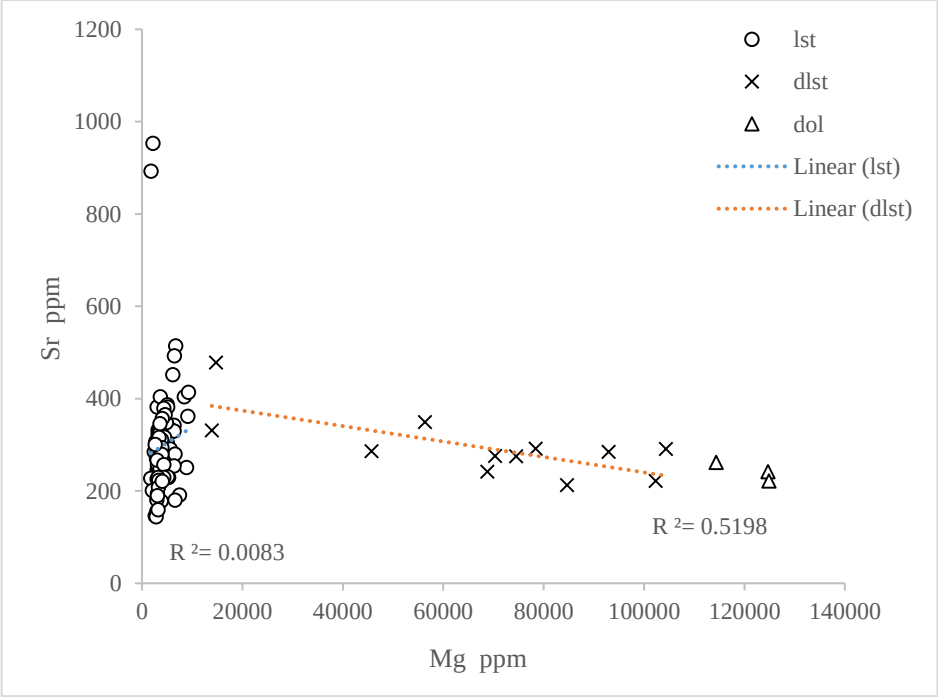

Figure 21. Scatter diagram showing the correlation of Sr with Mg, and a potentially high Sr aragonite precursor for the dolomite.

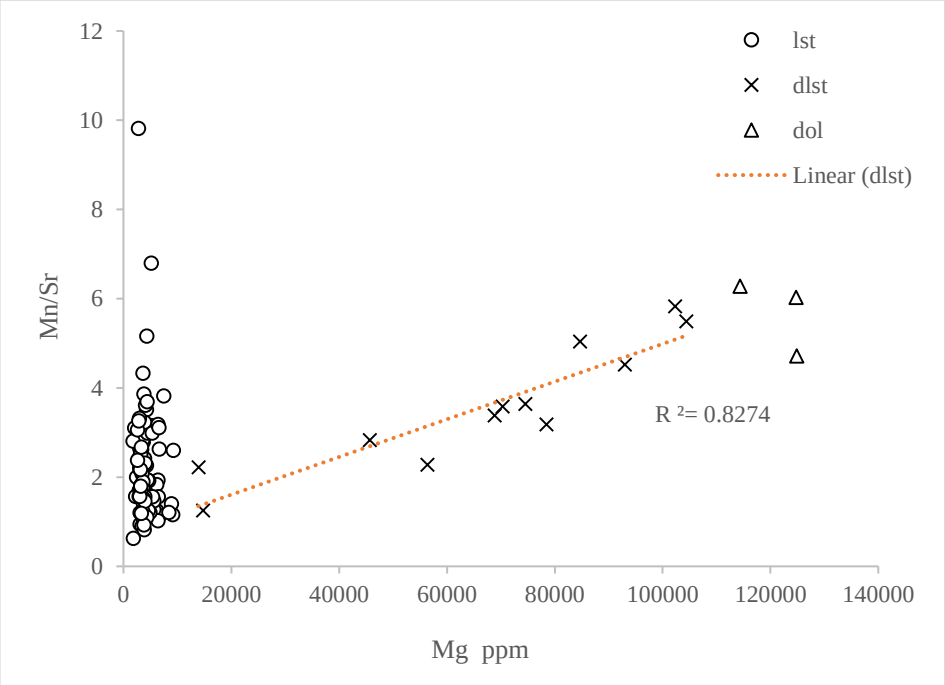

Figure 22. Scatter diagram showing the correlation of Mn/Sr ratios with Mg. The Mg and Mn/Sr ratios show a clear positive correlation with increasing dolomite composition.

The Sr content of most of samples range from 200 to 400 ppm. Two samples have higher Sr content (> 800 ppm), which should be used with caution. The Sr content of dolostone and dolomitic limestone are more concentrated than limestone (Figure 21).

With the increase of dolomite, the Mg content rises, too. The Mg contents of limestone are between 1715 to 9220 ppm. As for dolomitic limestone, the Mg is between 13,890 to 104,354 ppm, whereas the Mg content of dolostone samples can reach 124,854 ppm. The correlation between Sr and Mg is poor in limestone, but it is obvious and negative in dolomitic limestone (R^2=0.5198; Figure 21).

4.4 Stable Carbon and Oxygen Isotopes

Stable carbon and oxygen isotope compositions of the Green Point section carbonates are listed in Appendix 1 and illustrated in Figures 23–26. The $\delta^{13}C$ values ranges from -6.44‰ to +0.33‰, with an average of -2.37‰. The $\delta^{13}C$ values of the limestone samples are much more dispersed than those of the dolomitic limestone. The $\delta^{13}C$ values of dolostone are around -2‰. The $\delta^{18}O$ values are more concentrated than $\delta^{13}C$ values that vary from -8.63‰ to -5.67‰, and the average value is -7.54‰. The $\delta^{18}O$ values of dolostone are more positive than those of the limestone and dolomitic limestone. There is no obvious correlation between $\delta^{13}C$ and $\delta^{18}O$ values (Figure 23).

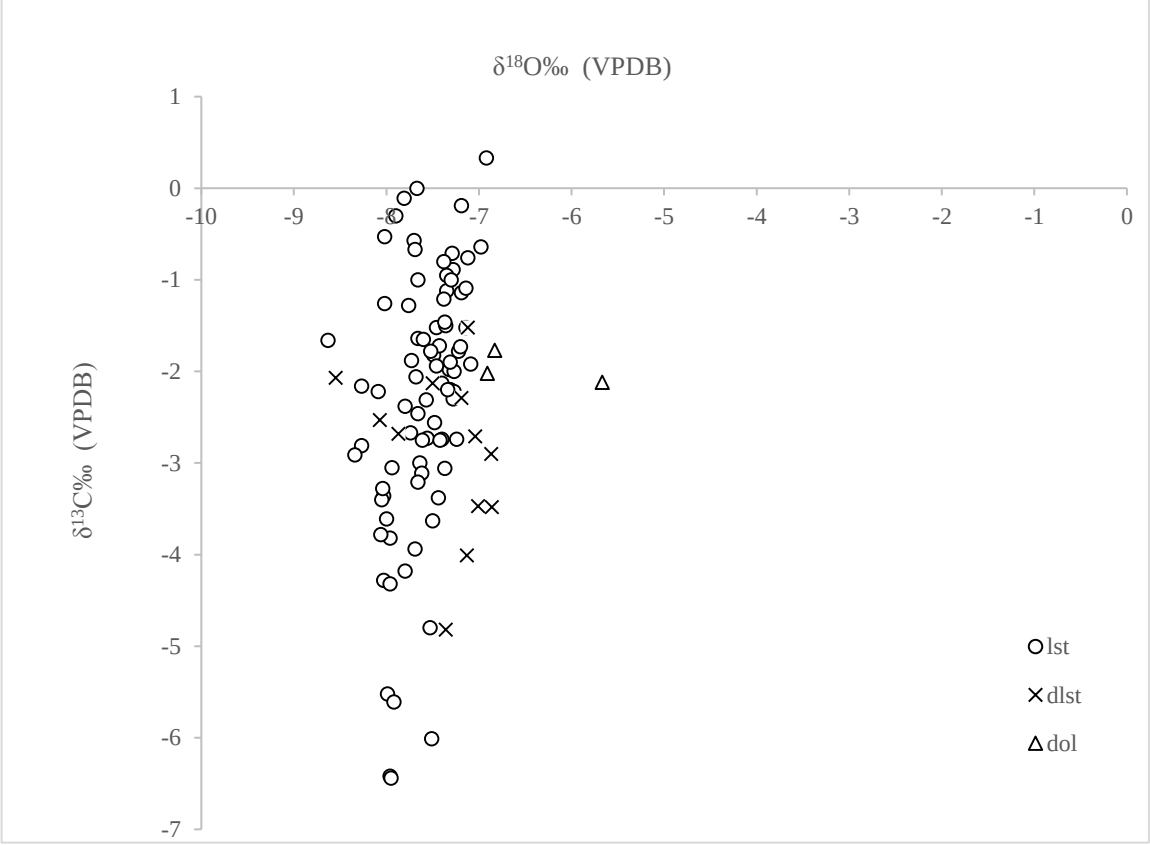

Figure 23. Plot of $\delta^{13}C$ and $\delta^{18}O$ values. The carbon isotope values are more scattered than the oxygen isotope ones.

The $\delta^{13}C$ values show no correlation with Mn/Sr ratios (Figure 24). The Mn/Sr ratio increases with dolomitization, and all the Mn/Sr ratios are lower than 8.0 except for one sample. The $\delta^{13}C$ values show no correlation with Mg content in limestone samples, either. However, dolomitization increases Mg content (Figure 25). The dolomitic samples also have high Fe content and relatively high carbon isotope values (Figure 26).

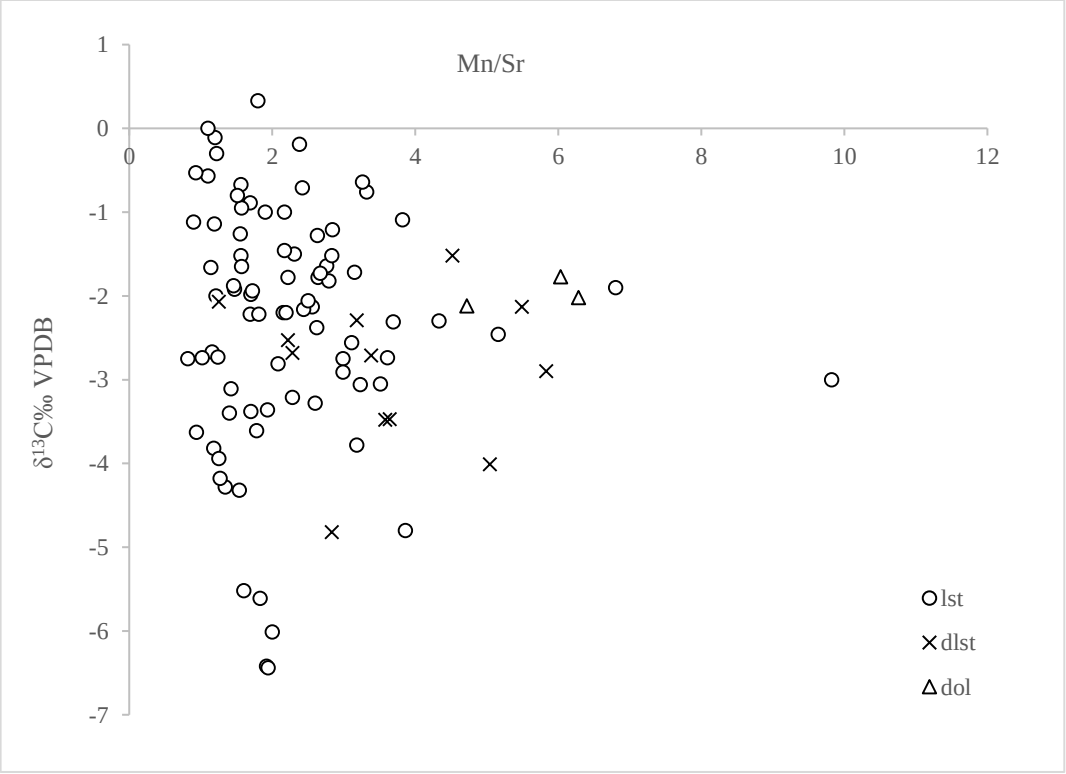

Figure 24. Plot of $\delta^{13}C$ values and Mn/Sr ratios.

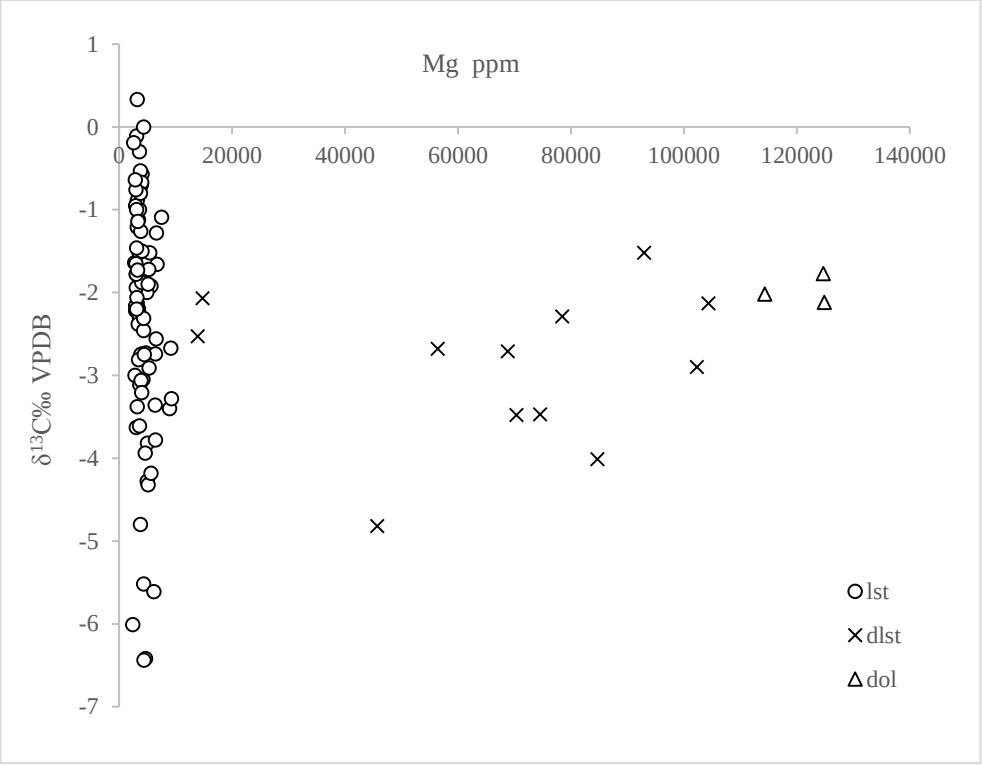

Figure 25. Plot of $\delta^{13}C$ values and Mg.

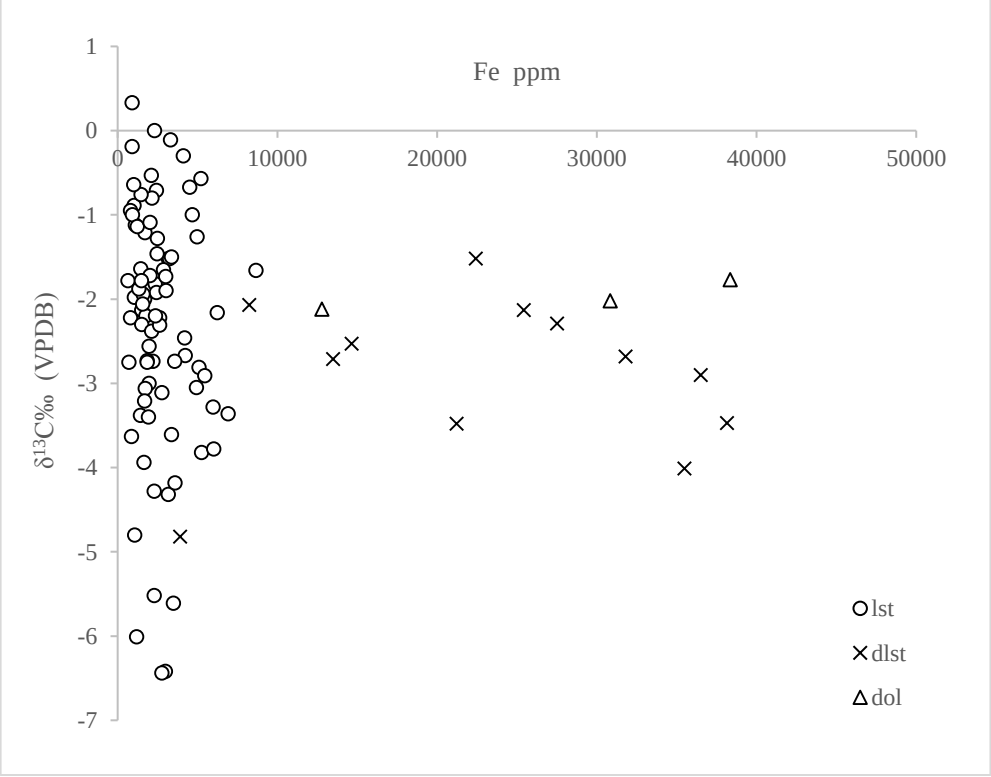

Figure 26. Plot of $\delta^{13}C$ values and Fe.

4.5 Chemostratigraphy

Based on sample horizon, we built stable carbon isotope profiles for the Green Point section (Figure 27; the top eighty-two results are from Azmy et al., 2014). It records the change of stable carbon isotope values from the top of the Furongian Series of the Cambrian to the Tremadocian of the Ordovician.

Stable carbon isotope compositions below the Ordovician GSSP fluctuate but remain essentially invariantly negative. Carbon isotope values fluctuate at the bottom of the succession. There is a significant negative carbon isotope excursion between 85 m and 90 m, with a nadir of -6.44 ‰. Carbon isotope values fluctuate between -5 ‰ to -3 ‰ within the next 7m. Then, carbon isotope values increase to around 0 ‰ at around 111 m and subsequently decrease to -4.8 ‰ at around 123 m. Then, the $\delta^{13}C$ values fluctuate between -3 ‰ to +1 ‰ over the next 35 m. There is a big negative stable carbon isotope excursion associated with the Ordovician GSSP, with a nadir of -4.7 ‰. After the Cambrian–Ordovician boundary $\delta^{13}C$ values rapidly increase to +0.6 ‰ (Figure 27).

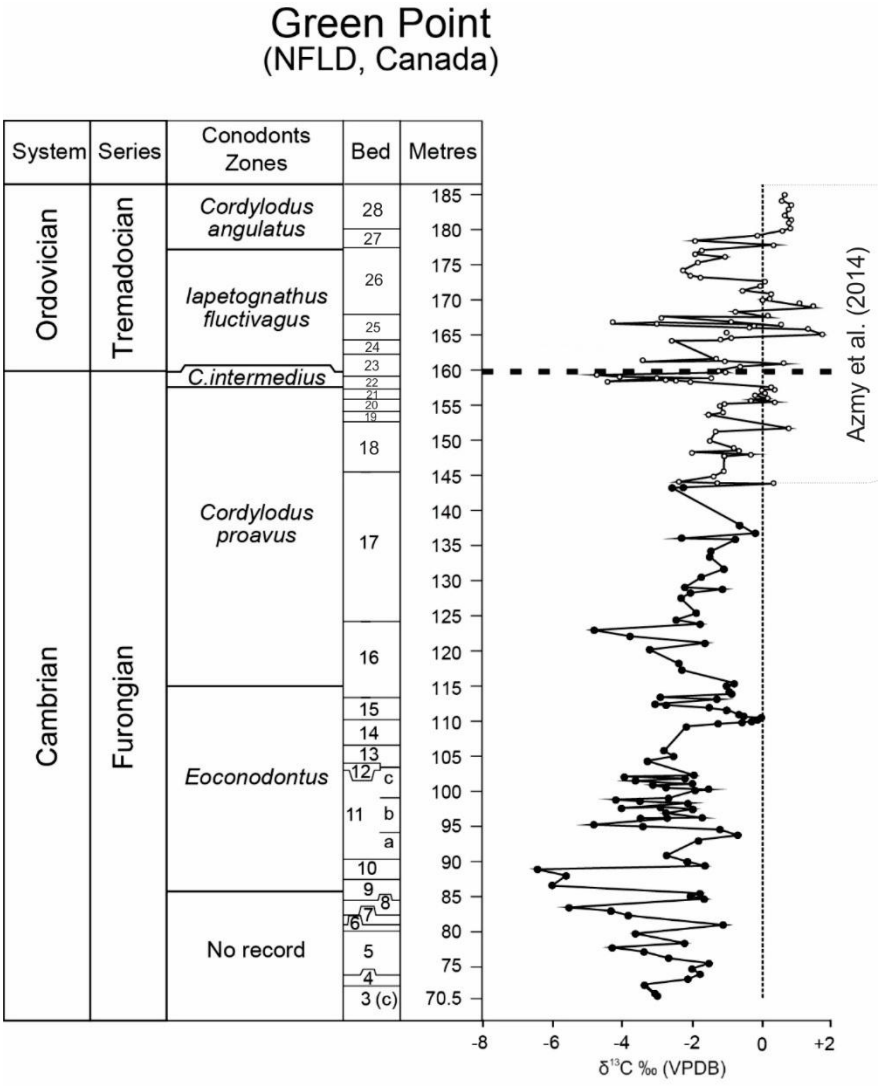

Figure 27. Carbon isotope chemostratigraphy of the Green Point section carbonates.

Chapter 5

Discussion

5.1 Evaluation of Sample Preservation

The carbon isotopes of whole rock may be used as proxy of original seawater carbon composition (Kaufman and Knoll, 1995; Brand et al., 2011). However, diagenesis can change the texture, mineralogy and original chemistry of carbonate and then the $\delta^{13}C_{carb}$ values may reflect the composition of the diagenetic fluid instead of the original and ambient seawater (Brand and Veizer, 1980, 1981). Therefore, carbonate samples should pass screening tests evaluating their post-depositional diagenesis and alternation before reconstructing carbon isotope profiles (cf., Brand et al., 2011). The earliest diagenetic alteration of carbonate may occur right after deposition when the carbonate was exposed to the marine water in which it formed and associated organisms may change the uppermost parts of the deposits (e.g., Swart, 2015). During the burial process and after uplift and exposure to vadose meteoric solutions, the original deposits may stay in a different chemical environment where further diagenesis may take place (e.g., Chilingar et al., 1967; Brand and Veizer, 1980; Williams et al., 1985).

The first method of testing for diagenesis is to evaluate the texture of the samples. Textural alternation usually occurs during transformation from a metastable phase to a more stable one (Brand and Veizer, 1980). During diagenesis, the content of sparry calcite increases because calcite spar as cement was precipitated in void spaces from pore fluids during the cementation process, and fine-grained calcite was converted to coarser-grained mosaic calcite by neomorphism (Williams et al., 1985). At Green Point, however, most of the examined samples are micritic limestone. Graded bedding and quartz replacement are

observed in a few samples. Although calcite spar precipitated as cement in fractures, fractures are not common in the samples from Green Point. Based on petrographic evaluation, most of the samples are micrite showing insignificant recrystallization and cement is not widely observed indicating, overall, relatively good preservation of the whole rock material.

Dull cathodoluminescence may indicate relative good preservation, whereas bright luminescence results from post-depostional alternation (e.g., Rush and Chafetz, 1990; Machel and Burton, 1991). However, cathodoluminescence in carbonates can be activated by high concentrations of Mn and quenched by high concentrations of Fe (Machel and Burton, 1991). Therefore, altered carbonate may have dull luminescence because of high concentration of Fe and well preserved samples may show bright luminescence due to high Mn content (Rush and Chafetz, 1990). Accordingly, cathodoluminescence observation by itself is insufficient for evaluating the preservation status of carbonate samples. Indeed, it should be complemented by additional screening tests (Brand et al., 2011; Azmy et al., 2014). At Green Point, samples show dull, dull-red, and bright-red-orange cathodoluminescence. As is shown in Table 3, 13 samples show dull cathodoluminescence containing high Fe and Mn content. 66 samples illustrate dull-red cathodoluminescence with less Fe and Mn contents compared with dull samples. The Fe content in bright-red-orange group is the lowest but Mn concentration is higher than the dull-red group. Therefore, cathodoluminescence of the carbonate samples at Green Point are basically dominated by contents of Fe and Mn that cannot be used as an equivocal indicator of preservation of samples.

Trace elemental ions such as Mg^{2+}, Mn^{2+}, Sr^{2+}, and Fe^{2+} can be incorporated into carbonate minerals in several ways, but only substitution for Ca^{2+} in the $CaCO_3$ lattice can be utilized for quantitative studies (Brand and Veizer, 1980; Veizer, 1983). Meteoric water contains less Sr^{2+}, but more Mn^{2+} and Fe^{2+}. $\delta^{18}O$ and probably $\delta^{13}C_{carb}$ values in meteoric water are more negative than those of seawater. Therefore, the diagenetic process would lead to enrichment of Mn^{2+} and Fe^{2+} and depletion of Sr^{2+}, ^{18}O, and ^{13}C in the diagenetic product. In contrast, the Mg^{2+} content can either increase or decrease depending on the original carbonate mineral (Brand and Veizer, 1980). Therefore, the changes of trace elements are important tracers because they can reflect the degree of post-depositional diagenesis and carbonate alteration.

Table 3. Chemical features of the three cathodoluminescence groups

Group		**Fe ppm**	**Mn ppm**	**Mn/Sr**	**$\delta^{13}C$ ‰**	**$\delta^{18}O$ ‰**
Dull	N	13	13	13	12	12
	Ave	26016	1105	4.23	-2.59	-7.00
	Min	4131	443	1.07	-4.01	-7.87
	Max	38351	1644	6.28	-1.52	-5.67
Dull-red	N	66	66	66	59	59
	Ave	3309	530	1.82	-2.27	-7.66
	Min	704	226	0.63	-6.01	-8.63
	Max	14657	1496	3.51	+0.33	-6.92
Bright-red-orange	N	29	29	29	27	27
	Ave	2124	802	3.15	-2.5	-7.5
	Min	658	396	1.51	-6.44	-8.00
	Max	419	2015	9.82	-0.64	-6.98

Both Sr and Mn are sensitive elements of post-depositional diagenesis. Sr^{2+} is easily leached from the carbonate lattice by meteoric water, while Mn^{2+} can be easily absorbed from diagenetic water into the carbonate lattice during post-depositional diagenesis (e.g., Brand and Veizer, 1980; Gilleaudeau and Kah, 2013). Since Sr and Mn elements have

opposite directional components with post-depositional diagenesis, the Mn/Sr ratio is a suitable geochemical proxy to evaluate the degree of alteration of marine carbonates (Kaufman and Knoll, 1995). The isotopic composition can represent the original sedimentary environment if the Mn/Sr ratio is lower than 3 and the diagenetic effect is considered negligible if the Mn/Sr ratio is less than 10 (Kaufman and Knoll, 1995). At Green Point, Mn/Sr ratios of samples are all less than 10, and 72 of them are less than 3, indicating that the carbonate are indeed well preserved. Moreover, Mn and Sr are poorly correlated (R^2=0.006). Consequently, this suggests that near-primary stable carbon isotope compositions are preserved in our samples.

In contrast, the oxygen isotope composition is much more sensitive in carbonates than carbon isotopes which are rock-buffered, because of the high water-rock ratios in meteoric diagenesis (e.g., Brand and Veizer, 1981; Banner and Hanson,1990; Knauth and Kennedy, 2009). The diagenetic fluids that fill the pores of rocks are enriched in ^{16}O, and will lower the $\delta^{18}O$ values of the carbonate during diagenesis (e.g., Jacobsen and Kaufman, 1999; Knauth and Kennedy, 2009). Generally, samples that were affected by post-sedimentary diagenesis would have more negative $\delta^{18}O$ values, and if the $\delta^{18}O$ values are lower than -10 ‰, the carbonate might have been altered (Kaufman and Knoll,1995; Lang et al., 2016). In this research, $\delta^{18}O$ values of all the samples range from -5.67 ‰ to -8.63 ‰ and they do not show significant correlation with $\delta^{13}C_{carb}$ values (Figure 23).

Carbon isotope values in carbonate sediment and rock may not closely reflect the depositional environment as they can react with meteoric pore water during diagenesis leading to positive or negative variations (Walter et al. 1993; Hu and Burdige 2007). The stable carbon isotope values of dolomitic limestone and dolostone have a narrower range

than of the limestone indicating dolomite was deposited in a shallow marine environment and subsequently influenced by meteoric water. However, the carbon isotope values show poor correlation with oxygen isotope values, Fe, Mn, Sr, and Mn/Sr all indicating good preservation of the carbonates at Green Point.

In summary, diagenesis of the limestone is negligible based on poor correlation of trace elements and stable isotopes. $\delta^{13}C$ signatures are considered reliable to reconstruct carbon isotope profile recording the original chemical features of seawater in the Late Cambrian sediments at Green Point. However, dolomitic limestone and dolostone may have altered in the shallow environment and suffered from more post-depositional alternation because of the slight correlation between trace elements and stable isotopes. Therefore, the carbon isotope values of dolomitic limestone and dolostone should be used with caution in chemostratigraphic reconstructions.

5.2 Stable Carbon Isotope Chemostratigraphy

Ripperdan (1992) found that sea level, conodont biozones and inorganic carbon isotope values changed synchronously within the Cambrian–Ordovician interval at Black Mountain, Australia. At the Green Point section, the carbon isotope values fluctuate through the whole section and they do not show clear correlation with conodont zones (Figure 27). During the Furongian Series of the late Cambrian in Australia, three sea level events are recorded in the sequence, and they all correspond to decreases in carbon isotope values (Ripperdan et al., 1992; Miller et al., 2015). At Green Point, the strata under the Cambrian–Ordovician boundary were deposited continuously in deep water and with no evidence of any significant stratigraphic breaks (Barnes, 1988). However, carbon isotope values decrease concomitantly with three regressions. The Red Tops Lowstand, the first regression event, is located at the base of *E. notchpeakensis* which corresponds to a large negative carbon isotope excursion (Miller et al., 2015). The Lange Ranch regression corresponds to the base of the *C. proavus* Zone that in turn corresponds to the middle carbon isotope excursion in the Green Point Section where $\delta^{13}C$ values drop from -0.8 ‰ to -4.8 ‰ (Ripperdan et al., 1992). The last regression event was the Basal House Lowstand that is marked by the beginning of the *C. intermedius* Zone, with $\delta^{13}C$ values decreasing from around 0 ‰ to -4.3 ‰ below the Ordovician GSSP (Azmy et al., 2014; Miller et al., 2015).

The negative carbon isotope excursion at the top of the *Cordylodus intermedius* Zone marks the Cambrian–Ordovician boundary (Azmy et al., 2014). In the lower part of the *C. proavus* Zone, there is a negative carbon isotope excursion with a decrease to -4.8 ‰. This excursion is termed the Top of the Cambrian Excursion (TOCE; Zhu el al., 2006). At the

base of the *Eoconodontus notchpeakensis* Zone, there is another big negative excursion followed by a smaller negative excursion. Ripperdan (2002) named this large negative carbon isotope excursion the Hellnmaria-Red Tops Boundary (HERB) carbon isotope excursion. Moreover, Landing (2010, 2011) confirmed that the HERB carbon isotope excursion is lower than the TOCE and corresponds to the FAD of *Eoconodontus notchpeakensis* (Figure 28).

5.3 Correlation

The GSSP of the Cambrian–Ordovician boundary was located at Green Point, western Newfoundland, Canada by the International Working Group on the Cambrian–Ordovician Boundary (COBWG) in 1999 and approved by the International Subcommission on Ordovician Stratigraphy (ISOS), the Commission on Stratigraphy, and by the International Union of Geological Sciences in the following year (Cooper et al., 2001). During its 25 years of investigation, the COBWG inspected many candidate sections in different countries, such as Kazakhstan, China, Australia, Scandinavia, Britain and North America. From this work, many papers were published and some of them also reported stable carbon isotope results.

Table 4 illustrates the sections where the HERB carbon isotope excursion has been found. Although strata were deposited in different environments of different depths, the amplitude of the HERB carbon isotope excursion is also different. The HERB carbon isotope excursion always shows up in the *Eoconodontus* Zone or below the *Cordylodus proavus* Zone (Figure 28). In inorganic records, the HERB carbon isotope excursion at Quebrada De La Flecha in Argentina was found without a conodont record and its nadir is -5.6 ‰ (Sial et al., 2008). The section at Baltica in Sweden has an organic carbon isotope record, and the nadir of the carbon isotope excursion is -30.5 ‰ and was also found without a conodont record (Terfelt et al., 2014). Hence, the HERB carbon isotope excursion can be found in both organic and inorganic carbon isotope records and in sections with/without substantiating conodont records.

Table 4. The sections were the HERB carbon isotope excursion was found (?: the location of HERB carbon isotope excursion is not sure).

No.	Location	Country	Source Material	Nadir of $\delta^{13}C$ ‰	Conodont Zone	Source
1	Black Mountain	Australia	carb	-3.5	Middle of *Econodontus*	Ripperdan et al., 1992
2	Dayangcha	North China	carb	-0.5	Base of *Eoconodontus*	Ripperdan et al., 1993
3	Lawson Cove	U.S.A.	carb	-1.5	Base of *Eoconodontus*	Ripperdan and Miller, 1995; Miller et al., 2006
4	Green Point (Ordovician GSSP)	Canada	carb	No record		Cooper et al., 2001
5	Cerro La Silla	Argentina	carb	-2.5	Below *Cordylodus proavus*	Buggisch et al., 2003
6	Quebrada De La Flecha	Argentina	carb	-5.6	No Conodont record	Sial et al., 2008
7	Kalpin	China	carb	-2?	No Conodont record	Jing et al., 2008
8	Kulyumbe River	Siberia	carb	-1?	Below *Cordylodus proavus*	Kouchinsky et al., 2008
9	Sneakover Pass	U.S.A.	carb	-1.0	Middle of *Eoconodontus notchpeakensis*	Miller et al., 2011
10	Sevier Lake Corral	U.S.A.	carb	-0.8	Top of *Eoconodontus notchpeakensis*	Miller et al., 2011
11	Quebrada De Juan Pobre	Argentina	carb	-1.9	No Conodont record	Sial et al., 2013
12	Baltica	Sweden	org	-30.5	No Conodont record	Terfelt et al., 2014

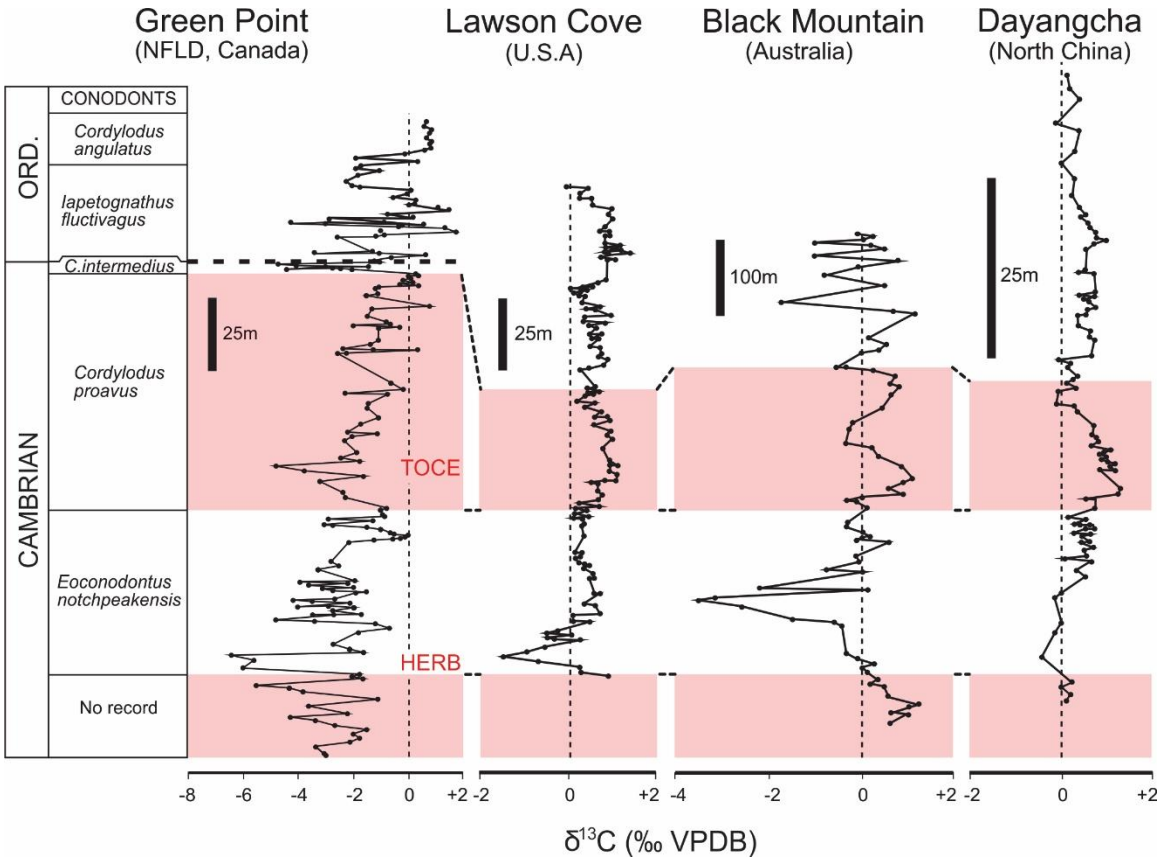

Figure 28. HERB carbon isotope excursion correlates with other sections covering the Cambrian–Ordovician interval: (A) Green Point section at western Newfoundland, Canada covering the Ordovician GSSP and Cambrian–Ordovician interval; (B) section at Lawson Cove, the United States of America (Ripperdan and Miller, 1995; modified from Miller et al., 2006); (C) section at Black Mountain, Australia (modified from Ripperdan et al., 1992); (D) section in Dayangcha, China (modified from Ripperdan et al., 1993).

Chapter 6

Conclusions

The carbonate samples below the Cambrian–Ordovician boundary are micritic or near-micritic limestone with minor dolomitic limestone and dolostone. They are determined to be in primary to near-primary conditions based on multiple screening tests, and stable carbon isotopes are deemed a reliable chemostratigraphic proxy.

Carbon isotope compositions below the Ordovician GSSP at Green Point, Newfoundland, Canada have fluctuated but remained essentially invariantly negative. They do not synchronously change with conodont biozones. However, the $\delta^{13}C_{carb}$ values reveal the TOCE in the uppermost Furongian series Stage 10, and the HERB carbon isotope excursion, with a nadir of -6.44 ‰, at the base of the *Eoconodontus notchpeakensis* Zone.

Carbon isotope chemostratigraphy may facilitate the correlation of intercontinental and intracontinental sequences. A large negative carbon isotope excursion found below the Cambrian–Ordovician boundary at Green Point, Newfoundland correlates well with the HERB carbon isotope excursion in the United States of America, Australia, Siberia, Argentina, and North China. Moreover, this correlation is achieved without an adequate record of conodonts, and thus carbon isotope chemostratigraphy can refine global stratigraphic correlations.

References

Azmy, K., Stouge, S., Brand, U., Bagnoli, G., & Ripperdan, R. (2014). High-resolution chemostratigraphy of the Cambrian–Ordovician GSSP; enhanced global correlation tool. *Palaeogeography, Palaeoclimatology, Palaeoecology*, *409*, 135–144. doi:10.1016/j.palaeo.2014.05.010

Babcock, L. E., Peng, S., Geyer, G., & Shergold, J. H. (2005). Changing perspectives on Cambrian chronostratigraphy and progress toward subdivision of the Cambrian System. *Geosciences Journal [Seoul]*, *9*(2), 101–106.

Banner, J. L., & Hanson, G. N. (1990). Calculation of simultaneous isotopic and trace element variations during water-rock interaction with applications to carbonate diagenesis. *Geochimica et Cosmochimica Acta*, *54*(11), 3123–3137. doi:10.1016/0016-7037(90)90128-8

Barnes, C. R. (1988). The proposed Cambrian – Ordovician global Boundary stratotype and point (GSSP) in Western Newfoundland, Canada. *Geological Magazine*, (July), 381–414. https://doi.org/10.1017/S0016756800013042

Brand, U., Logan, A., Bitner, M. A., Griesshaber, E., Azmy, K., & Buhl, D. (2011). What is the ideal proxy of Palaeozoic seawater chemistry? *Memoirs of The Association of Australasian Palaeontologists*, *41*, 9–24.

Brand, U., & Veizer, J. (1980). Chemical diagenesis of a multicomponent carbonate system; 1, Trace elements. *Journal of Sedimentary Petrology*, *50*(4), 1219–1236. doi:10.1306/212F7BB7-2B24-11D7-8648000102C1865D

Brand, U., & Veizer, J. (1981). Chemical diagenesis of a multicomponent carbonate system; 2, Stable isotopes. *Journal of Sedimentary Petrology*, *51*(3), 987–997. doi:10.1306/212F7DF6-2B24-11D7-8648000102C1865D

Buggisch, W., Keller, M., & Lehnert, O. (2003). Carbon isotope record of Late Cambrian to Early Ordovician carbonates of the Argentine Precordillera. *Palaeogeography, Palaeoclimatology, Palaeoecology, 195*(3–4), 357-373. doi:10.1016/S0031-0182(03)00365-1

Chilingar, G., Bissell, H., & Wolf, K. (1967). Diagenesis of Carbonate Rocks. In *Development in Sedimentology* (Vol. 8, pp. 179–322). Elsevier. https://doi.org/10.1016/S0070-4571(08)70844-6

Cooper, R. A., Nowlan, G. S., & Williams, S. H. (2001). Global stratotype section and point for base of the Ordovician system. *Episodes*, *24*(1), 19–28. Retrieved from http://www.scopus.com/scopus/inward/record.url?eid=2-s2.0-0035630931&partnerID=40&rel=R5.6.0

Dickson, J. D. (1966). Carbonate identification and genesis as revealed by staining. *Journal of Sedimentary Petrology*, *36*(2), 491–505. doi:10.1306/74D714F6-2B21-11D7-8648000102C1865D

Fritz, P., & Smith, D. W. (1970). The isotopic composition of secondary dolomites. *Geochimica et Cosmochimica Acta*, *34*(11), 1161–1173.

Gilleaudeau, G. J., & Kah, L. C. (2013). Carbon isotope records in a Mesoproterozoic epicratonic sea; carbon cycling in a low oxygen world. *Precambrian Research*, *228*, 85–101. doi:10.1016/j.precamres.2013.01.006

Hu, X., & Burdige, D. J. (2007). Enriched stable carbon isotopes in the pore waters of carbonate sediments dominated by sea grasses; evidence for coupled carbonate dissolution and reprecipitation. *Geochimica et Cosmochimica Acta*, *71*(1), 129–144. doi:10.1016/j.gca.2006.08.043

Jacobsen, S. B., & Kaufman, A. J. (1999). The Sr, C and O isotopic evolution of Neoproterozoic seawater. *Chemical Geology*, *161*(1–3), 37–57. doi:10.1016/S0009-2541(99)00080-7

James, N. P. (1981). Megablocks of calcified algae in the Cow Head breccia, western Newfoundland; vestiges of a Cambro–Ordovician platform margin. *Geological Society of America Bulletin*, *92*(11), 799–811.

James, N. P., & Stevens, R. K. (1986). Stratigraphy and correlation of the Cambro–Ordovician Cow Head group, western Newfoundland. Ottawa: Energy, Mines, and Resources Canada: Available in Canada from Canadian Govt. Pub. Centre, Supply and Services Canada, 1986.

Jing, X., Deng, S., Zhao, Z., Lu, Y., & Zhang, S. (2008). Carbon isotope composition and correlation across the Cambrian–Ordovician boundary in Kalpin Region of the Tarim Basin, China. *Science in China. Series D: Earth Sciences*, *51*(9), 1317–1329. doi:10.1007/s11430-008-0093-5

Johnson, K. S., Berelson, W. M., Coale, K. H., Coley, T. L., Elrod, V. A., Fairey, W. R., & Nowicki, J. L. (1992). Manganese flux from continental margin sediments in a transect through the oxygen minimum. *Science*, *257*(5074), 1242–1245.

Kaufman, A. J., & Knoll, A. H. (1995). Neoproterozoic variations in the C-isotopic composition of seawater; stratigraphic and biogeochemical implications. *Precambrian Research, 73*(1–4), 27–49. doi:10.1016/0301-9268(94)00070-8

Knauth, L. P., & Kennedy, M. J. (2009). The late Precambrian greening of the Earth. *Nature [London]*, *460*(7256), 728–732. doi:10.1038/nature08213

Kouchinsky, A, Bengtson, S., Gallet, Y., Korovnikov, I., Runnegar, B., Shields, G., … Ziegler, K. (2008). The SPICE carbon isotope excursion in Siberia: a combined study of the upper Middle Cambrian–lowermost Ordovician Kulyumbe River section, northwestern Siberian Platform. *Geological Magazine, 145*(5), 609–622. https://doi.org/10.1017/S0016756808004913

Landing, E., Westrop, S. R., & MILLER, J. F. (2010). Globally practical base for the uppermost Cambrian (Stage 10): FAD of the conodont Eoconodontus notchpeakensis and the Housian (read "Lawsonian" as in abstract) Stage, p. 18. In O. Fatka and P. Budil (eds.), The 15th Field Conference of the Cambrian Stage Subdivision Working Group.

Landing, E., Westrop, S. R., & Adrain, J. M. (2011). The Lawsonian Stage; the Eoconodontus notchpeakensis (Miller, 1969) FAD and HERB carbon isotope excursion define a globally correlatable terminal Cambrian stage. *Bulletin of Geosciences [Praha]*, *86*(3), 621–640. doi:10.3140/bull.geosci.1251

Lang, X., Shen, B., Peng, Y., Huang, K., Lu, J., & Ma, H. (2016). Ocean oxidation during the deposition of basal Ediacaran Doushantuo cap carbonates in the Yangtze Platform, south China. *Precambrian Research, 281,* 253–268. doi:10.1016/j.precamres.2016.06.006

Lindholm, R. C., & Finkelman, R. B. (1972). Calcite staining; semiquantitative determination of ferrous iron. *Journal of Sedimentary Petrology*, *42*(1), 239–242

Machel, H. G., & Burton, E. A. (1991). Factors governing cathodoluminescence in calcite and dolomite and their implications for studies of carbonate diagenesis. *SEPM Short Course Notes, 25*, 37–57.

Miller, J. F., Ethington, R. L., Evans, K. R., Holmer, L. E., Loch, J. D., Popov, L. E., & ... Taylor, J. F. (2006). Research paper: Proposed stratotype for the base of the highest Cambrian stage at the first appearance datum of Cordylodus andresi, Lawson Cove section, Utah, USA. *Palaeoworld*, *15*(The Fourth International Symposium on the Cambrian System), *15*(3), 384–405. doi:10.1016/j.palwor.2006.10.017

Miller, J. F., Evans, K. R., Freeman, R. L., Ripperdan, R. L., & Taylor, J. F. (2011). Proposed stratotype for the base of the Lawsonian Stage (Cambrian Stage 10) at the first appearance datum of Econodontus notchpeakensis (Miller) in the House Range, Utah, USA. *Bulletin of Geosciences [Praha]*, *86*(3), 595–620. doi:10.3140/bull.geosci.1255

Miller, J. F., Ripperdan, R. L., Loch, J. D., Freeman, R. L., Evans, K. R., Taylor, J. F., & Tolbart, Z. C. (2015). Proposed GSSP for the base of Cambrian Stage 10 at the lowest occurrence of Eoconodontus notchpeakensis in the House Range, Utah, USA. *Annales De Paleontologie*, *101*(3), 199–211. doi:10.1016/j.annpal.2015.04.008

Palmer, A. R. (1977). Biostratigraphy of the Cambrian System; a progress report. *Annual Review of Earth and Planetary Sciences*, *5*, 13–33.

Ripperdan, R. L., Magaritz, M., & Kirschvink, J. L. (1993). Carbon isotope and magnetic polarity evidence for non-depositional events within the Cambrian–Ordovician boundary section near Dayangcha, Jilin Province, China. *Geological Magazine*, *130*(4), 443–452.

Ripperdan, R. L., Magaritz, M., Nicoll, R. S., & Shergold, J. H. (1992). Simultaneous changes in carbon isotopes, sea level, and conodont biozones within the Cambrian–Ordovician boundary interval at Black Mountain, Australia. *Geology*, *20*(11), 1039–1042. https://doi.org/10.1130/0091-7613(1992)020<1039:SCICIS>2.3.CO

Ripperdan, R. L., & Miller, J. F. (1995). Carbon isotope ratios from the Cambrian–Ordovician boundary section at Lawson Cove, Ibex area, Utah. *Field Trip Guidebook - Pacific Section, Society of Economic Paleontologists and Mineralogists*, *77*, 129–132.

Ripperdan, R. L. (2002). The HERB event; end of the Cambrian carbon cycle paradigm? *Abstracts with Programs - Geological Society of America*, *34*(6), 413.

Rush, P. F., & Chafetz, H. S. (1990). Fabric-retentive, non-luminescent brachiopods as indicators of original delta (super 13) C and delta (super 18) O composition; a test. *Journal of Sedimentary Petrology*, *60*(6), 968–981. doi:10.1306/D4267659-2B26-11D7-8648000102C1865D

Scotese, C.R., 2002, http://www.scotese.com, (PALEOMAP website).

Sial, A. N., Peralta, S., Ferreira, V. P., Toselli, A. J., Acenolaza, F. G., Parada, M. A., & ... Pimentel, M. M. (2008). Upper Cambrian carbonate sequences of the Argentine Precordillera and the Steptoean C-Isotope positive excursion (SPICE). *Gondwana Research*, *13*(4), 437–452. doi:10.1016/j.gr.2007.05.001

Sial, A. N., Peralta, S., Gaucher, C., Toselli, A. J., Ferreira, V. P., Frei, R., & ... Silva Pereira, N. (2013). High-resolution stable isotope stratigraphy of the upper Cambrian and Ordovician in the Argentine Precordillera; carbon isotope excursions and correlations. *Gondwana Research*, *24*(1), 330–348. doi:10.1016/j.gr.2012.10.014

Suchecki, R. K., & Hubert, J. F. (1984). Stable isotopic and elemental relationships of ancient shallow-marine slope carbonates, Cambro–Ordovician Cow Head Group, Newfoundland; implications for fluid flux. *Journal of Sedimentary Petrology*, *54*(4), 1062–1080.

Swart, P. K. (2015). The geochemistry of carbonate diagenesis; the past, present and future. *Sedimentology*, *62*(5), 1233–1304. doi:10.1111/sed.12205

Terfelt, F., Bagnoli, G., & Stouge, S. (2012). Re-evaluation of the conodont Iapetognathus and implications for the base of the Ordovician system GSSP. *Lethaia*, *45*(2), 227–237. doi:10.1111/j.1502-3931.2011.00275.x

Terfelt, F., Eriksson, M. E., & Schmitz, B. (2014). The Cambrian–Ordovician transition in dysoxic facies in Baltica - diverse faunas and carbon isotope anomalies. *Palaeogeography, Palaeoclimatology, Palaeoecology*, *394*, 59–73. https://doi.org/10.1016/j.palaeo.2013.11.021

Veizer, J. (1983). Chemical diagenesis of carbonates; theory and application of trace element technique. *SEPM Short Course*, 103.1.

Williams, H., James, N. P., & Stevens, R. K. (1985). Humber Arm Allochthon and nearby groups between Bonne Bay and Portland Creek, western Newfoundland. *Paper - Geological Survey of Canada, 85–1A*, 399–406.

Walter, L. M., Bischof, S. A., Patterson, W. P., Lyons, T. W., O'Nions, R. K., Gruszczynski, M., Coleman, M. L. (1993). Dissolution and recrystallization in modern shelf carbonates: evidence from pore water and solid phase chemistry [and discussion]. *Philosophical Transactions of the Royal Society of London. Series A: Physical and Engineering Sciences*, *344*(1670), 27–36. https://doi.org/10.1098/rsta.1993.0072

Zhang, T., Chu, X., Zhang, Q., Feng, L., & Huo, W. (2003). Variations of sulfur and carbon isotopes in seawater during the Doushantuo Stage in late Neoproterozoic. *Chinese Science Bulletin*, *48*(13), 1375–1380. doi:10.1360/02wd0434

Zhu, M., Babcock, L. E., & Peng, S. (2006). Research paper: Advances in Cambrian stratigraphy and paleontology: Integrating correlation techniques, paleobiology,

taphonomy and paleoenvironmental reconstruction. *Palaeoworld*, *15*(The Fourth International Symposium on the Cambrian System), 217–222. doi:10.1016/j.palwor.2006.10.016

Appendix

Appendix 1 Trace element and isotopic compositions of Green Point samples including cathodoluminescence and petrography.

Sample ID	Bed	Depth*	Mean $\delta^{13}C_{VPDB}$ of Peaks	Mean $\delta^{18}O_{VPDB}$ of Peaks	Ca	Mg	Sr	Mn	Fe	Mn/Sr	Cathodoluminescence	Petrography
		m	‰	‰	ppm	ppm	ppm	ppm	ppm			
GP H1	3(c)	70.50	-3	-7.64	392236	2764	205	2015	1966	9.82	Bright-orange	Limestone
GP H2	3(c)	71.10	-3.05	-7.94	390785	4215	312	1096	4947	3.51	Dull-red	Limestone
GP H3	3(c)	72.30	-3.36	-8.03	388637	6363	342	660	6929	1.93	Dull-red	Limestone
GP H4	4	73.20	-2.13	-7.5	290646	104354	291	1596	25437	5.49	Dull	Dolomitic limestone
GP H5	5	73.95	-1.77	-6.83	270302	124698	242	1458	38351	6.03	Dull	Dolostone
GP H6	5	74.65	-2.02	-6.91	280673	114327	262	1644	30850	6.28	Dull	Dolostone
GP H7	5	75.50	-1.52	-7.12	302059	92941	285	1288	22436	4.52	Dull	Dolomitic limestone
GP H8	5	76.30	-2.67	-7.74	385872	9128	362	421	4239	1.16	Dull-red	Limestone
GP H9	5	77.20	-3.38	-7.44	391843	3157	323	548	1427	1.70	Bright-orange	Limestone
GP H10	5	77.75	-4.28	-8.03	390043	4957	306	412	2296	1.34	Dull-red	Limestone
GP H11	5	78.45	-2.22	-8.09	392109	2891	218	367	2639	1.69	Dull-red	Limestone
GP H12	5	79.80	-3.63	-7.5	391977	3023	382	359	873	0.94	Dull-red	Limestone
GP H13	7	81.10	-1.12	-7.35	391615	3385	323	291	1116	0.90	Dull-red	Limestone
GP H13 1	7	81.10			391382	3618	404	433	4131	1.07	Dull	Limestone

Sample ID	Bed	Depth*	Mean $\delta^{13}C_{VPDB}$ of Peaks	Mean $\delta^{18}O_{VPDB}$ of Peaks	Ca	Mg	Sr	Mn	Fe	Mn/Sr	Cathodoluminescence	Petrography
GP H14	8	82.50	-3.82	-7.96	389980	5020	387	455	5253	1.18	Dull-red	Limestone
GP H14 1	8	82.50			388867	6133	452	567	6055	1.25	Dull-red	Limestone
GP H15	8	83.10	-4.32	-7.96	389918	5082	382	588	3172	1.54	Dull-red	Limestone
GP H16	8	83.60	-5.52	-7.99	390687	4313	379	605	2292	1.60	Dull-red	Limestone
GP H17	9	84.90	-1.66	-8.63	388324	6676	514	585	8663	1.14	Dull-red	Limestone
GP H18	9	85.30	-2.07	-8.55	380261	14739	478	598	8243	1.25	Dull-red	Dolomitic limestone
GP H19	9	85.70	-1.78	-7.22	392013	2987	245	646	658	2.64	Bright-orange	Limestone
GP H20	9	86.90	-6.01	-7.51	392604	2396	285	572	1194	2.00	Dull-red	Limestone
GP H21	10	88.30	-5.61	-7.92	388889	6111	330	605	3494	1.83	Dull-red	Limestone
GP H22-1	10	89.20	-6.42	-7.96	390320	4680	323	621	2989	1.92	Bright-orange	Limestone
GP H22-2	10	89.20	-6.44	-7.95	390612	4388	309	600	2767	1.94	Bright-orange	Limestone
GP H23	10	89.80	-1.64	-7.66	392259	2741	307	846	1443	2.76	Bright-red	Limestone
GP H24	10	90.30	-2.13	-7.4	391806	3194	251	644	1514	2.56	Dull-red	Limestone
GP H25	11	91.30	-2.74	-7.4	390940	4060	240	866	2220	3.61	Bright-red	Limestone
GP H25-1	11	91.30			392804	2196	953	1496	3898	1.57	Dull-red	Limestone
GP H25-2	11	91.30			388590	6410	493	770	2301	1.56	Bright-orange	Limestone
GP H26	11	93.40	-1.82	-7.49	391384	3616	245	684	2361	2.79	Bright-red	Limestone
GP H26 1	11	93.40			390748	4252	355	803	2107	2.26	Bright-red	Limestone

Sample ID	Bed	Depth*	Mean $\delta^{13}C_{VPDB}$ of Peaks	Mean $\delta^{18}O_{VPDB}$ of Peaks	Ca	Mg	Sr	Mn	Fe	Mn/Sr	Cathodoluminescence	Petrography
GP H27	11	94.20	-0.71	-7.29	391132	3868	260	628	2437	2.42	Bright-red	Limestone
GP H28	11	95.00	-1.21	-7.38	391800	3200	234	664	1714	2.84	Bright-red	Limestone
GP H29	11	95.50	-4.82	-7.36	349307	45693	286	810	3918	2.83	Dull-red	Dolomitic limestone
GP H30	11	96.40	-3.4	-8.05	386121	8879	251	350	1927	1.40	Dull-red	Limestone
GP H31A	11	96.70	-2.71	-7.04	326202	68798	242	816	13488	3.38	Dull	Dolomitic limestone
GP H31B	11	96.70	-3.47	-7.01	320466	74534	275	1001	38151	3.64	Dull	Dolomitic limestone
GP H31B 1	11	96.70			393200	1800	893	563	2409	0.63	Dull-red	Limestone
GP H32	11	96.80	-1.72	-7.43	389783	5217	296	933	2030	3.15	Dull-red	Limestone
GP H33	11	97.40	-2.73	-7.56	390289	4711	277	342	1844	1.24	Dull-red	Limestone
GP H33 1	11	97.40			386590	8410	404	487	7511	1.21	Dull-red	Limestone
GP H34	11	97.70	-2.75	-7.42	391188	3812	275	226	704	0.82	Dull-red	Limestone
GP H35	11	97.90	-1.98	-7.32	391318	3682	244	415	1045	1.70	Dull-red	Limestone
GP H36	11	98.15	-4.01	-7.13	310345	84655	213	1072	35500	5.04	Dull	Dolomitic limestone
GP H37	11	98.30	-2.9	-6.87	292704	102296	222	1296	36523	5.83	Dull	Dolomitic limestone
GP H38	11	98.80	-2.12	-5.67	270146	124854	222	1047	12801	4.72	Dull	Dolostone
GP H39	11	99.20	-3.48	-6.86	324686	70314	276	988	21221	3.58	Dull	Dolomitic limestone
GP H40	11	99.40	-4.18	-7.8	389402	5598	334	423	3604	1.27	Dull-red	Limestone
GP H41	11	99.60	-2.68	-7.87	338635	56365	349	796	31806	2.28	Dull	Dolomitic limestone

Sample ID	Bed	Depth*	Mean $\delta^{13}C_{VPDB}$ of Peaks	Mean $\delta^{18}O_{VPDB}$ of Peaks	Ca	Mg	Sr	Mn	Fe	Mn/Sr	Cathodoluminescence	Petrography
GP H42	11	100.75	-1.92	-7.09	389380	5620	291	429	2423	1.47	Dull-red	Limestone
GP H43	11	100.90	-1.52	-7.14	389614	5386	251	393	3183	1.56	Dull-red	Limestone
GP H44	11	101.10	-2.74	-7.24	388614	6386	330	336	3583	1.02	Dull-red	Limestone
GP H45	11	101.50	-3.11	-7.62	391342	3658	254	360	2783	1.42	Dull-red	Limestone
GP H45 1	11	101.50			391188	3812	178	537	3109	3.02	Dull-red	Limestone
GP H46	11	101.70	-2	-7.27	390128	4872	348	422	1694	1.21	Dull-red	Limestone
GP H47	11	102.15	-3.61	-8	391403	3597	272	484	3369	1.78	Bright-red	Limestone
GP H48	11	102.35	-2.2	-7.31	391603	3397	267	573	1775	2.15	Bright-red	Limestone
GP H49	11	102.45	-2.22	-7.27	391814	3186	332	600	813	1.81	Dull-red	Limestone
GP H50	11	102.70	-3.94	-7.69	390406	4594	365	458	1651	1.25	Dull-red	Limestone
GP H51	11	102.90	-1.94	-7.46	391982	3018	286	491	1589	1.72	Dull-red	Limestone
GP H52	13	105.00	-3.28	-8.04	385780	9220	414	1074	5980	2.60	Dull-red	Limestone
GP H53	13	105.70	-2.53	-8.07	381110	13890	331	733	14657	2.22	Dull-red	Dolomitic limestone
GP H54	13	106.50	-2.81	-8.27	391604	3396	332	690	5091	2.08	Dull-red	Limestone
GP H55	15	110.00	-2.16	-8.27	392092	2908	181	442	6236	2.44	Dull-red	Limestone
GP H56	15	110.50	-1.26	-8.02	391206	3794	314	486	4983	1.55	Dull-red	Limestone
GP H57	15	110.70	-0.57	-7.7	390966	4034	357	391	5224	1.10	Dull-red	Limestone
GP H58	15	110.80	-0.3	-7.9	391442	3558	327	399	4125	1.22	Dull-red	Limestone

Sample ID	Bed	Depth*	Mean $\delta^{13}C_{VPDB}$ of Peaks	Mean $\delta^{18}O_{VPDB}$ of Peaks	Ca	Mg	Sr	Mn	Fe	Mn/Sr	Cathodoluminescence	Petrography
GP H59	15	111.10	-0.11	-7.81	391944	3056	306	366	3305	1.20	Dull-red	Limestone
GP H60	15	111.30	0	-7.67	390703	4297	277	305	2307	1.10	Dull-red	Limestone
GP H61	15	111.50	-0.53	-8.02	391232	3768	316	295	2107	0.93	Dull-red	Limestone
GP H62	15	111.80	-0.67	-7.69	391045	3955	318	498	4525	1.56	Dull-red	Limestone
GP H64	15	112.40	-1	-7.66	391430	3570	346	657	4685	1.90	Dull-red	Limestone
GP H65	15	112.80	-1.52	-7.46	391489	3511	298	843	3262	2.83	Dull-red	Limestone
GP H66	15	113.20	-2.75	-7.61	390558	4442	317	947	1855	2.99	Bright-orange	Limestone
GP H67	16	113.30	-3.06	-7.37	391109	3891	311	1006	1722	3.23	Bright-red	Limestone
GP H68	16	114.00	-1.28	-7.76	388415	6585	280	738	2501	2.63	Bright-red	Limestone
GP H69	16	114.30	-2.91	-8.34	389701	5299	229	686	5453	2.99	Dull-red	Limestone
GP H70	16	114.90	-0.89	-7.28	391829	3171	267	453	1034	1.69	Dull-red	Limestone
GP H71	16	115.00	-0.95	-7.35	392112	2888	270	425	818	1.57	Dull-red	Limestone
GP L72	16	116.00	-1	-7.3	391926	3074	257	558	936	2.17	Dull-red	Limestone
GP L73	16	116.30	-0.8	-7.38	391237	3763	263	396	2158	1.51	Bright-red	Limestone
GP L74	16	118.30	-2.3	-7.28	391441	3559	249	1076	1518	4.33	Bright-red	Limestone
GP L75	16	119.25	-2.38	-7.8	391634	3366	316	829	2140	2.62	Bright-red	Limestone
GP L76	16		-1.88	-7.73	391042	3958	294	428	1338	1.46	Dull-red	Limestone
GP L77	16	121.30	-3.21	-7.66	391041	3959	279	635	1698	2.28	Bright-red	Limestone

Sample ID	Bed	Depth*	Mean $\delta^{13}C_{VPDB}$ of Peaks	Mean $\delta^{18}O_{VPDB}$ of Peaks	Ca	Mg	Sr	Mn	Fe	Mn/Sr	Cathodoluminescence	Petrography
GP L78	16	122.20	-1.65	-7.6	392029	2971	267	419	2867	1.57	Dull-red	Limestone
GP L79	16	123.20	-3.78	-8.06	388602	6398	254	807	6011	3.18	Dull-red	Limestone
GP L79 1	16	123.20			393285	1715	227	637	2150	2.81	Dull-red	Limestone
GP L79 2	16	123.20			392983	2017	201	623	2387	3.10	Dull-red	Limestone
GP L80	16	124.15	-4.8	-7.53	391249	3751	229	885	1063	3.86	Bright-red	Limestone
GP L81	17	125.00	-1.78	-7.52	391985	3015	226	501	1488	2.22	Bright-red	Limestone
GP L82	17	125.60	-2.46	-7.66	390678	4322	257	1328	4195	5.16	Bright-red	Limestone
GP L83	17	126.60	-1.9	-7.31	389873	5127	231	1570	3036	6.80	Bright-red	Limestone
GP L84	17	128.75	-2.31	-7.57	390672	4328	229	846	2638	3.69	Bright-red	Limestone
GP L85	17	129.50	-2.06	-7.68	391845	3155	229	571	1574	2.50	Dull-red	Limestone
GP L86	17	130.10	-1.14	-7.19	391716	3284	223	266	1225	1.19	Dull-red	Limestone
GP L87	17	130.35	-2.2	-7.34	391942	3058	194	425	2371	2.19	Dull-red	Limestone
GP L88	17	131.80	-1.73	-7.2	391738	3262	208	555	3017	2.67	Bright-orange	Limestone
GP L88 1	17	131.80			392409	2591	301	922	762	3.06	Dull	Limestone
GP L89	17	133.00	-1.09	-7.14	387532	7468	191	729	2040	3.82	Bright-red	Limestone
GP L90	17	134.80	-1.5	-7.36	390972	4028	221	511	3384	2.31	Dull-red	Limestone
GP L91	17	135.60	-1.46	-7.37	391918	3082	190	412	2466	2.17	Dull-red	Limestone
GP L92	17	137.35	-0.76	-7.12	392066	2934	156	519	1475	3.32	Dull-red	Limestone

Sample ID	Bed	Depth*	Mean $\delta^{13}C_{VPDB}$ of Peaks	Mean $\delta^{18}O_{VPDB}$ of Peaks	Ca	Mg	Sr	Mn	Fe	Mn/Sr	Cathodoluminescence	Petrography
GP L93	17	137.50	-2.29	-7.19	316573	78427	292	929	27515	3.18	Dull	Dolomitic limestone
GP L94	17	138.25	-0.19	-7.19	392414	2586	146	348	910	2.38	Dull-red	Limestone
GP L95	17	139.35	-0.64	-6.98	392176	2824	144	468	1004	3.26	Bright-orange	Limestone
GP L96	17	144.90	-2.56	-7.48	388456	6544	180	559	1974	3.11	Dull-red	Limestone
GP L97	18	145.45	+0.33	-6.92	391842	3158	159	286	904	1.80	Dull-red	Limestone

*Depth is estimated based on measurements from *James & Stevens, 1986*.